PHYSICAL REVIEW D **82,** 043510 (2010)

CMB in a box: Causal structure and the Fourier-Bessel expansion

L. Raul Abramo*

Instituto de Física, Universidade de São Paulo, CP 66318, 05314-970, São Paulo, Brazil
and Department of Astrophysical Sciences, Princeton University, Peyton Hall, Princeton, New Jersey 08544, USA

Paulo H. Reimberg and Henrique S. Xavier

Instituto de Física, Universidade de São Paulo, CP 66318, 05314-970, São Paulo, Brazil
(Received 10 May 2010; published 6 August 2010)

This paper makes two points. First, we show that the line-of-sight solution to cosmic microwave anisotropies in Fourier space, even though formally defined for arbitrarily large wavelengths, leads to position-space solutions which only depend on the sources of anisotropies inside the past light cone of the observer. This foretold manifestation of causality in position (real) space happens order by order in a series expansion in powers of the visibility $\gamma = e^{-\mu}$, where μ is the optical depth to Thomson scattering. We show that the contributions of order γ^N to the cosmic microwave background (CMB) anisotropies are regulated by spacetime window functions which have support only inside the past light cone of the point of observation. Second, we show that the Fourier-Bessel expansion of the physical fields (including the temperature and polarization momenta) is an alternative to the usual Fourier basis as a framework to compute the anisotropies. The viability of the Fourier-Bessel series for treating the CMB is a consequence of the fact that the visibility function becomes exponentially small at redshifts $z \gg 10^3$, effectively cutting off the past light cone and introducing a finite radius inside which initial conditions can affect physical observables measured at our position $\vec{x} = 0$ and time t_0. Hence, for each multipole ℓ there is a discrete tower of momenta $k_{i\ell}$ (not a continuum) which can affect physical observables, with the smallest momenta being $k_{1\ell} \sim \ell$. The Fourier-Bessel modes take into account precisely the information from the sources of anisotropies that propagates from the initial value surface to the point of observation—no more, no less. We also show that the physical observables (the temperature and polarization maps), and hence the angular power spectra, are unaffected by that choice of basis. This implies that the Fourier-Bessel expansion is the optimal scheme with which one can compute CMB anisotropies.

DOI: 10.1103/PhysRevD.82.043510 PACS numbers: 98.80.−k, 98.70.Vc, 98.80.Es

I. INTRODUCTION

The cosmic microwave background (CMB) is the earliest, cleanest observation that reveals what the Universe looked like at the very beginning. A remarkable string of observations of the CMB temperature fluctuations over the last 20 years, most notably by COBE-DMR [1] and WMAP [2–4], has shown that the typical initial conditions of the Universe when it was under 400 000 years old can be characterized by extreme homogeneity and isotropy, only slightly perturbed by small, $\mathcal{O}(10^{-5})$ fluctuations with a nearly scale-invariant spectrum. More recently, the small degree of polarization that is imprinted on the CMB radiation by anisotropic Thomson scattering has also started to become detectable [5–7], and may hold the key to unravel the mystery of the birth of our Universe—see, e.g., [8–11].

The remarkable success of the CMB as probably the most powerful tool in observational Cosmology can also be traced to the simplicity of its underlying mechanisms: Thomson scattering and linear perturbation theory. The basic theory, which is an application of the relativistic radiative transfer equations [12], was initially developed in connection with the CMB by Peebles and Yu [13], and the first to write down the full collisional Boltzmann equations for temperature and polarization were Bond and Efstathiou [14,15].

However, even if the main mechanisms driving acoustic oscillations in the baryon-photon fluid were basically understood early on, crucial features such as neutrinos, gravitational waves, spatial curvature and the effects of lensing on polarization remained puzzling. It was not until the 1990's that the theory reached full maturity, when the complete separation of radial and angular modes allowed by the use of spin angular momentum eigenfunctions for polarization cleared the way for our current understanding of CMB physics [16–24].

One particularly significant step forward was achieved with the line-of-sight solution to the collisional Boltzmann equations [25]. The idea is that photons travel along null geodesics, hence the comoving distance Δx between two successive collisions is equal to the conformal time interval $\Delta\eta$ between those collisions (as usual, we assume that the Born approximation is valid.) This means that, given a line of sight $\hat{n}$, we know that a photon detected at time η travelling along that line of sight was at the position $\vec{x}' = \hat{n}(\eta - \eta')$ at time η', if no collisions occurred between

*abramo@fma.if.usp.br

those times. The more general case of an ensemble of photons can be easily accommodated in this picture, since the probability that a photon scatters with free electrons is given in terms of the optical depth for Thomson scattering, which to a very good approximation is a smooth function of time, $\mu(\eta)$. The final state of the ensemble is then obtained through integration over time of the sources of temperature and polarization anisotropies, appropriately weighted by the optical depth at each time.

The power of the line-of-sight integral solution is that it separates, as much as it is possible, the (free) propagation of photons from the ultimate sources of anisotropies (matter and metric perturbations)—so, it is similar in spirit to a Green's function for the temperature and polarization of an ensemble of photons. However, there is one feature of the generation of anisotropies which makes it impossible to completely separate the sources and the anisotropies: anisotropic Thomson scattering is itself a source of both temperature and polarization, so the process is, in some sense, nonlocal.

When photons scatter at a given place and time, the fluctuations in temperature and polarization that are generated as a consequence of those scatterings depend also on the quadrupole of the temperature and the polarization of the photons that were incident at that place and time. Therefore, the fact that those incident photons typically propagated to the location of the scattering from far away implies that the process is nonlocal—hence the line-of-sight solution is actually a set of integral equations, at least for the lowest multipoles ($\ell \leq 2$). The higher multipoles ($\ell \geq 3$), however, can be completely determined from the lowest multipoles, which makes the line-of-sight solution a vastly superior method compared to the usual hierarchy of Boltzmann equations. Of course, for the low multipoles the integral equations are impractical, and the preferred method to compute them is to revert back to the hierarchy of Boltzmann equations, which is then truncated at a relatively low multipole that is sufficient to accurately compute the multipoles $\ell \leq 2$.

Nevertheless, despite the fact that the generation of anisotropies is a nonlocal mechanism, it is still completely causal: photons propagate along light cones between scatterings (which are basically instantaneous within the cosmological time scales.) The main drive behind this work is to clarify how causality and nonlocality are manifested in the generation of the CMB. We are interested, in particular, in describing the generation of the CMB in position (real) space, since Fourier space can sometimes obfuscate the causal nature of the physical mechanisms.

We will show that, in position space, the nonlocal anisotropies can be resolved into explicitly causal pieces by iterating the integral line-of-sight equations. The smallness parameter in this perturbative expansion (which is reminiscent of the Dyson series of quantum electrodynamics [26]) is the *total* visibility $\gamma = e^{-\mu}$, where μ is the optical depth to Thomson scattering. The first term in that series corresponds to the last scattering of the photons before they were detected; the second term corresponds to the last two scatterings before detection; and so on.

In this series over the number of scatterings, causality is manifested at each order in terms of radial integrals corresponding to spacetime window functions which are only nonzero inside the past light cone (PLC) of the observation point. The spacetime dependence of the γ^N-order term is given in terms of integrals of $N+1$ spherical Bessel functions, which we demonstrate to have support only inside the PLC. The first term of the series, $\mathcal{O}(\gamma^1)$, corresponds simply to the Sachs-Wolfe (SW), Doppler and integrated Sachs-Wolfe (ISW) contributions to the temperature fluctuations from the last scattering [27], and evidently it is only nonzero at the surface of the light cone. The second-order terms for temperature and polarization carry the memory of the last two scatterings, and can be nonzero anywhere inside the volume of the PLC (not only on its surface). Figure 1 illustrates the structure of the light cones for one, two and three scatterings. Hence, we have shown that the line-of-sight integrals are actually *retarded* Green's functions for the temperature and polarization, and we found analytical expressions for them in position space.

The second result of this paper follows from this causal structure. The expansion in successive scatterings (or, equivalently, in orders of the visibility function) makes it clear that what matters for the CMB observables are not simply the source fields and the anisotropies as functions of position and time, $f(\vec{x}, \eta)$, but the fields multiplied by powers of the visibility, $\gamma(\eta)^N f(\vec{x}, \eta)$. Since the visibility vanishes for very early times (say, $z_i \gg 10^3$), for all prac-

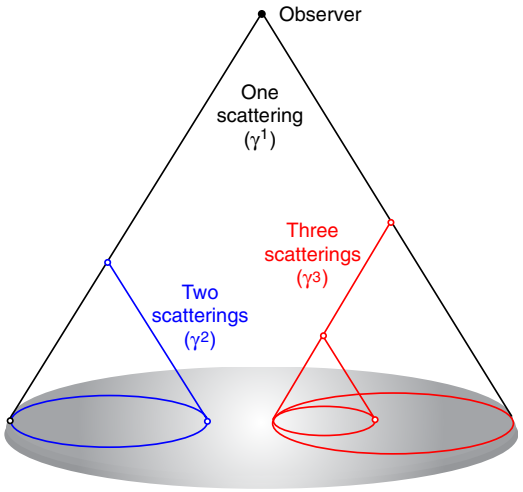

FIG. 1 (color online). Past light cones for photons experiencing one, two, and three scatterings since the time of decoupling from matter (denoted as the base of the cone.) The terms corresponding to these interactions are, respectively, of order γ^1, γ^2, and γ^3, where $\gamma = e^{-\mu}$ is the visibility.

tical purposes that have to do with the CMB, our PLC is cut off at $\eta_i = \eta(z_i)$, and all the sources are effectively zero outside the radius corresponding to that time (which in a typical flat ΛCDM model is approximately $r_i \approx 5H_0^{-1}$.)

The fact that the physical fields are exponentially suppressed at the boundaries of the PLC means that the best basis for expanding the fields, as well as the anisotropies, is not the Fourier basis, which is most convenient for plane waves in $\mathbb{R}^3$, but the Fourier-Bessel basis [28], which expands functions $f(\vec{x})$ inside a 3D sphere of finite radius R into spherical harmonics $Y_{\ell m}(\hat{x})$ and spherical Bessel functions $j_\ell(k_{i\ell}x)$, with $k_{i\ell}R$ being the ith root of j_ℓ. Both sets of basis functions are eigenvectors of the Laplacian operator in flat space, with eigenvalues $-\vec{k}^2$ or $-k_{i\ell}^2$, but they differ most significantly in that the Fourier-Bessel series establishes a discrete tower of momenta for each multipole ℓ, so that the smallest momentum mode is $k_{1\ell} \sim \ell/r_i$. Therefore, there is a clearly defined minimal mode that can contribute to CMB observables, and the modes above it are all discretized. The drawback is that, if the underlying fields are Gaussian in nature, the Fourier-Bessel modes, as opposed to the Fourier modes, are not statistically independent, so their covariance matrix is not diagonal. However, dynamics is one thing, statistics is another, and we will show how these issues can be separated so that we can easily recover angular power spectra which have precisely the same statistical properties as the power spectra computed in Fourier space.

The first part of this work takes an approach which is similar to that used to make constrained simulations of CMB temperature and polarization maps by Liguori, Matarrese, and Moscardini [29] and by Komatsu, Spergel, and Wandelt [30]—see also [31–33]. However, while those simulations make use of several approximation schemes in order to produce numerically viable codes, our expressions are exact and analytical. In particular, our results show that the transfer functions of [29,30] have an invariant (or geometrical) piece which is described by our spacetime window functions, so that the transfer functions can be obtained by integration of these window functions over time with some visibility function. Another work close in spirit to ours was done by Bashinsky and Bertshinger [34,35], who calculated the Green's function for the evolution of linear cosmological perturbations in position space but did not compute the Green's functions for the anisotropies.

A quick note on our conventions: the Fourier transform of a function $f(\vec{x})$ is $f(\vec{k}) = (2\pi)^{-3/2}\int d^3x e^{-i\vec{k}\cdot\vec{x}} f(\vec{x})$; unit vectors expressing lines-of-sight or other directions are denoted by a hat, so $\vec{x} = x\hat{x}$; the perturbed Friedman-Robertson-Walker metric is $ds^2 = a^2(\eta)[-(1+2\Phi)d\eta^2 + (1-2\Psi)d\vec{x}^2]$; and the relationship between the rotation matrices and the spin spherical harmonics is $D^\ell_{m,-s}(\alpha,\beta,\gamma\to 0) = \sqrt{4\pi/(2\ell+1)}Y^*_{\ell m}(\beta,\alpha)s$, so that ${}_sY^*_{\ell m} = (-1)^{m-s}{}_{-s}Y_{\ell,-m}$. Finally, everything we will say in this paper concerns scalar (spin-0) density perturbations—we will consider lensing and gravitational waves in future work.

II. CMB ANISOTROPIES IN A NUTSHELL

The main channel of electron-photon interactions during recombination is elastic Thomson scattering. The likelihood of a photon interacting with free electrons between times η_1 and η_2 can be determined in terms of the optical depth for Thomson scattering:

$$\mu(\eta_1,\eta_2) = \int_{\eta_1}^{\eta_2} d\eta a(\eta)\sigma_T n_e(\eta)X_e(\eta), \tag{1}$$

where $a(\eta)$ is the Friedman-Robertson-Walker scale factor, $\sigma_T = 6.65\times 10^{-25}$ cm^2 is the Thomson cross section, n_e is the total number density of electrons, and X_e is the ionized fraction. The probability per unit time that a photon observed at η_2 had last interacted at time η_1 is called the *visibility function*:

$$g(\eta_1,\eta_2) = \frac{d}{d\eta_1}e^{-\mu(\eta_1,\eta_2)}, \tag{2}$$

where $g(\eta_1,\eta_2)$ is a positive-definite function, normalized to unity if the limits are taken such that $\mu\to 0$ and $\mu\to\infty$ at late and early times, respectively. It is customary to define the visibility function today simply by $g(\eta) = g(\eta,\eta_0)$. In this work we will also define the *total visibility* (or unscattered fraction) as:

$$\gamma(\eta_1,\eta_2) = e^{-\mu(\eta_1,\eta_2)}. \tag{3}$$

Notice that the *total* visibility is the probability that a photon will *not* scatter after η_1 before it is detected at η_2, and in fact we defined it such that it is related to the visibility *function* by $g(\eta_1,\eta_2) = d/d\eta_1[\gamma(\eta_1,\eta_2)]$.

At very early times, the optical depth is extremely large, so the Universe is effectively opaque and the visibility vanishes exponentially. Photons and electrons are interacting so often that the photons can spend enough time in some small region so that inelastic processes lead to thermalization with the electrons and, by extension, with the baryons. Hence, at very early times (much before recombination) the photon distribution $\Theta(\vec{x},\eta;\hat{l}) = \Delta T/T$ was essentially in equilibrium with baryonic matter, and only the monopole $\theta_0(\vec{x},\eta) = \int d^2\hat{l}/(4\pi)\Theta(\vec{x},\eta;\hat{l}) = \delta_\gamma/4$ was significant (here δ_γ is the density contrast of photons.)

However, as soon as recombination starts, the optical depth plummets, scatterings between photons and electrons become sparser, and as a result the radiation incident on any given scattering source can be increasingly anisotropic, since photons arriving to a scattering source from distant over- or underdense regions have different equilibrium temperatures. Thomson scattering with anisotropic radiation then generates polarization (and vice versa), and the process becomes quite intricate.

Let us assume for a moment that the photons decoupled from matter instantly, at some time η_R, and propagated freely from that time down to our detectors at $\vec{x} = 0$, η_0. Then direct integration of the geodesic equation (with the help of the Born approximation) tells us that the temperature from a given line of sight $\hat{l}$ in fact reflects the density, gravitational potential and velocities at the position $\vec{x}_l = (\eta_0 - \eta_R)\hat{l}$ and time η_R, as well as any time-varying gravitational potentials along that light cone [27]:

$$\Theta(\vec{x} = \vec{0}, \eta_0; \hat{l}) = [\theta_0 + \Phi + \hat{l} \cdot \vec{\nabla} V_b](\vec{x}_l, \eta_R) + \int_{\eta_R}^{\eta_0} d\eta (\Phi' + \Psi')(\vec{x}_l, \eta_R), \quad (4)$$

where V_b is the baryon velocity potential. This equation shows that the primary (and ultimate) sources of anisotropies are the inhomogeneities in the matter and metric fields of the Universe (θ_0, Φ, Ψ, and V_b.)

Now let us relax the assumption of instant recombination, but still require that the photons did not scatter again after decoupling. This is the same as saying that the visibility function is not assumed to be proportional to a delta function $\delta(\eta - \eta_R)$ anymore, but is still a positive, normalized function, highly peaked at the time of recombination. In that case the photons will carry the average temperature of the location where they last scattered, along with the local gravitational potential Φ and baryon velocity V_b, and this signal will be affected by the time-varying metric perturbations only after that last scattering. Considering that the probability that a photon will scatter between some time η' and the some time η is given by the visibility function $g(\eta', \eta)$, but the probability that they will *not* scatter anymore after the time η' is given by the *total* visibility $\gamma(\eta', \eta)$, the line-of-sight solution becomes

$$\Theta^{(1)}(\vec{0}, \eta; \hat{l}) = \int_0^{\eta} d\eta' \{ g(\eta', \eta)[\theta_0 + \Phi + \hat{l} \cdot \vec{\nabla} V_b] \times (\vec{x}_l, \eta') + \gamma(\eta', \eta)(\Phi' + \Psi')(\vec{x}_l, \eta') \}, \quad (5)$$

where now $\vec{x}_l = \Delta\eta \hat{l}$, with $\Delta\eta = (\eta - \eta')$. The superscript 1 is used to denote that this contribution is linear with in the total visibility γ (as well as the visibility function, $g = d\gamma/d\eta$).

Equation (5) tells us that, in a first approximation, to obtain the temperature anisotropies one should simply average the sources over the PLC $\vec{x}_l$, with weights given either by the visibility function (for the SW and Doppler terms) or by the total visibility (for the ISW term.) This approximation would correspond to the "one scattering" diagram of Fig. 1.

The next level of complexity leads to polarization. Let us assume that the approximation above is still true for the temperature, but that photons can scatter a second time after decoupling. Then, the incident radiation at the location of that scattering will in general be anisotropic, simply because of the inhomogeneities in the Universe at the time of decoupling. If that incident radiation has a quadrupole, then Thomson scattering will excite the linear polarization degrees of freedom of the Stokes parameters Q and U. Clearly, then, polarization is of at least second order in the visibility, since it enters once when the photons first decouple from the matter, and then a second time when the anisotropic ensemble of photons scatter off free electrons, generating the polarization.

The assumptions above are too simplistic, of course: as we go back in time the number of scatterings per Hubble time rise steeply, which means that the problem that must be solved is one of successive scatterings of a polarized, inhomogeneous and anisotropic temperature distribution which is, moreover, coupled to baryons and dark matter.

The result of taking into account the anisotropy and polarization of the incident radiation in Thomson scattering leads to corrections to Eq. (5) and to the generation of polarization [8,10,11,14,23,36,37]. The polarization at any given point in space and time is best given in terms of the (dimensionless) spin +2 eigenstate combination:

$$\frac{Q + iU}{4I} \equiv P(\vec{x}, \eta; \hat{l}) = \sqrt{\frac{3}{40\pi}} \int_0^{\eta} d\eta' g(\eta', \eta)[\theta_2(\vec{x}', \eta') - \sqrt{6} p_2(\vec{x}', \eta')], \quad (6)$$

where θ_2 and p_2 are the quadrupole of the temperature and of the polarization, which we will define in more detail below. The integration above is along the line of sight $\hat{l}$, so the sources that contribute to the polarization at the position $\vec{x}$ come from $\vec{x}' = \vec{x} + \Delta\eta \hat{l}$, at times η'. A similar equation applies for the temperature anisotropies, and it should be clear that these equations are only a closed set with the addition of the perturbed Einstein equations, as well as the continuity and Euler equations for baryons, dark matter and neutrinos—see, e.g., [8,11,16].

It should be evident from the symmetries of the problem that it is natural to break this system of equations into spherical coordinates with respect to the lines of sight $\hat{l}$ around an observer at the origin. For temperature, which is a scalar under rotations, the spherical harmonic decomposition reads

$$\Theta(\vec{x}, \eta; \hat{l}) = \sum_{\ell m} \Theta_{\ell m}(\vec{x}, \eta) Y_{\ell m}(\hat{l}). \quad (7)$$

Polarization, on the other hand, is such that the Stokes parameters Q and U change sign if we perform a rotation of π over the line of sight, which means that they are components of a spin-2 field. In fact, the complex combination in Eq. (6) was chosen such that it is a spin +2 eigenstate. Hence, polarization in this form can be expanded in terms of the spin +2 eigenfunctions, or spin +2 spherical harmonics [22,23]:

$$P(\vec{x}, \eta; \hat{l}) = \sum_{\ell \geq 2, m} P_{\ell m}(\vec{x}, \eta)\, {}_2Y_{\ell m}(\hat{l}). \tag{8}$$

In Fourier space the dependence on $\hat{l}$ can be easily isolated, since $e^{i\vec{k}\cdot\vec{x}'} = e^{i\vec{k}\cdot\vec{x}} e^{i\Delta\eta \vec{k}\cdot\hat{l}}$. We then employ Rayleigh's expansion, $e^{i\vec{k}\cdot\vec{x}} = 4\pi \sum_{\ell m} i^\ell j_\ell(kx) Y^*_{\ell m}(\hat{k}) Y_{\ell m}(\hat{x})$, and the line-of-sight integrals determining anisotropies can be written in the form [23,25]:

$$\Theta_{\ell m}(\vec{x}, \eta) = 4\pi i^\ell \int \frac{d^3k}{(2\pi)^{3/2}} e^{i\vec{k}\cdot\vec{x}} Y^*_{\ell m}(\hat{k}) \theta_\ell(\vec{k}, \eta), \tag{9}$$

$$P_{\ell m}(\vec{x}, \eta) = 4\pi i^\ell \int \frac{d^3k}{(2\pi)^{3/2}} e^{i\vec{k}\cdot\vec{x}} Y^*_{\ell m}(\hat{k}) p_\ell(\vec{k}, \eta), \tag{10}$$

where the temperature and polarization momenta, θ_ℓ and p_ℓ, are derived from the geodesic equation for photons in the presence of Thomson scattering:

$$\theta_\ell(\vec{k}, \eta) = \theta^{(1)}_\ell(\vec{k}, \eta) + \frac{1}{4} \int_0^\eta d\eta' g(\eta', \eta) [\theta_2(\vec{k}, \eta') - \sqrt{6} p_2(\vec{k}, \eta')] \left[1 + 3 \frac{\partial^2}{\partial (k\Delta\eta)^2}\right] j_\ell(k\Delta\eta), \tag{11}$$

$$\theta^{(1)}_\ell(\vec{k}, \eta) = \int_0^\eta d\eta' \left\{ g(\eta', \eta) \left[\theta_0(\vec{k}, \eta') + \Phi(\vec{k}, \eta') + V_b(\vec{k}, \eta') \frac{\partial}{\partial \eta} \right] + \gamma(\eta', \eta)(\Phi' + \Psi') \times (\vec{k}, \eta') \right\} j_\ell(k\Delta\eta), \tag{12}$$

$$p_\ell(\vec{k}, \eta) = -\frac{3}{4} \sqrt{\frac{(\ell+2)!}{(\ell-2)!}} \int_0^\eta d\eta' g(\eta', \eta) [\theta_2(\vec{k}, \eta') - \sqrt{6} p_2(\vec{k}, \eta')] \frac{j_\ell(k\Delta\eta)}{(k\Delta\eta)^2}. \tag{13}$$

For the derivation of the polarization term for the temperature quadrupole, including the radial function, see also [38].

Therefore, in this form the structure of the interactions is more clear than in the hierarchy of Boltzmann equations, but at the price of stating the problem in terms of integro-differential equations. This complexity is just apparent, though, since all higher-order source terms have angular momenta $\ell \leq 2$, and if we solve for the low ones, all the higher multipoles can be computed with the help of the integrals above [25].

III. CMB IN POSITION SPACE AND CAUSALITY

The integral equations (11)–(13) should be solved, in principle, for all momenta $\vec{k}$ so that the temperature and polarization anisotropies in Eqs. (9) and (10) can be computed. This includes the modes with $k \ll H_0$, which correspond to arbitrarily large wavelengths and can contribute to the zero mode of the fluctuations. Now, does this mean that perturbations outside the horizon can contribute anything to the CMB that we observer? In fact, they do not: we will show that the temperature and polarization of the CMB which are observed at any spacetime point $(\vec{x}, \eta)$ only include information from inside the PLC of that point. This statement is true at each order in the visibility γ, and for each spherical mode (ℓ, m).

The first step to recover the causal structure which underlies the temperature and polarization is to go from Fourier space back to position space. The most direct way to go back to position space without relinquishing the spherical harmonic decomposition is to use the fact that the Fourier- and position-space harmonics are simply related by a Hankel transform:

$$f(\vec{x}) = \sum_{LM} f_{LM}(x) Y_{LM}(\hat{x}), \qquad f(\vec{k}) = \sum_{LM} f_{LM}(k) Y_{LM}(\hat{k}), \tag{14}$$

$$f_{LM}(x) = \sqrt{\frac{2}{\pi}} i^L \int_0^\infty dk k^2 j_L(kx) f_{LM}(k), \qquad f_{LM}(k) = \sqrt{\frac{2}{\pi}} (-i)^L \int_0^\infty dx x^2 j_L(kx) f_{LM}(x). \tag{15}$$

If $f(\vec{x})$ is a real function, then the harmonic coefficients obey the conjugation relations $f^*_{\ell m}(r) = (-1)^m f_{\ell,-m}(r)$ in position space and $f^*_{\ell m}(r) = (-1)^{\ell+m} f_{\ell,-m}(r)$ in Fourier space.

The relations above between $f_{LM}(x)$ and $f_{LM}(k)$ are quite remarkable: they tell us that the spherical harmonic phases do not mix at all. This is a consequence [39] of the fact that angular momentum is the same operator in position and in Fourier space, $\mathbf{L} = i\vec{x} \times \vec{\partial}_x = i\vec{k} \times \vec{\partial}_k$. It is worth noting that apparently this technique were first used in Cosmology in connection with redshift space distortions—see, e.g., [39–41]. In connection with the CMB, the spherical decomposition has been used in simulations [29,30], and as a tool to study polarization from clusters of galaxies by [38,42].

A. γ^1 term: $\Theta^{(1)}$ in position space

Now we can easily substitute the sources in terms of this spherical harmonic decomposition into $\theta^{(1)}_\ell$. In the following subsections we show how this prescription can be extended to the remaining terms in the expressions (11) and (13).

Let us then express the monopole θ_0, newtonian potential Φ and baryon velocity potential V_b in terms of spherical harmonics $Y_{LM}(\hat{x})$, and use them to compute the temperature anisotropies at our location (assuming that

we occupy the origin of the spherical coordinate system, at $\vec{x} = 0$), to first order in the visibility. Substituting the spherical harmonic decomposition in $\vec{x}$ into Eq. (12) for $\theta^{(1)}$, inserting that expression in Eq. (7) and integrating over $d^2\hat{k}$ (which makes $L = \ell$ and $M = m$), leads to

$$\Theta^{(1)}_{\ell m}(\vec{0}, \eta) = \frac{2}{\pi}\int_0^\infty dk k^2 \int_0^\eta d\eta' \int_0^\infty dx x^2 S_{\ell m}(x, \eta, \eta') \times j_\ell(k\Delta\eta) j_\ell(kx), \tag{16}$$

where we have collected the sources in the term

$$S_{\ell m}(x, \eta, \eta') = g(\eta', \eta)\Big[\theta_{0,\ell m}(x, \eta') + \Phi_{\ell m}(x, \eta') - V_{b,\ell m}(x, \eta')\frac{\partial}{\partial\eta'}\Big] + \gamma(\eta', \eta)(\Phi' + \Psi')_{\ell m}(x, \eta'). \tag{17}$$

Notice that we have defined the sources in an unusual way, including a factor of the visibility function for the Sachs-Wolfe and Doppler terms, and a factor of the total visibility for the integrated Sachs-Wolfe term. The matter and metric fields are actually just functions of (x, η'), but we include the extra dependence on η that comes from the visibility into the definition of the source term in order to simplify the notations.

Now the integral over k in Eq. (16) can be computed, and in fact that happens to be exactly the orthogonality condition for spherical Bessel functions:

$$\int_0^\infty dk k^2 j_\ell(kx) j_\ell(kx') = \frac{\pi}{2} x^{-2}\delta(x - x'). \tag{18}$$

This implies that Eq. (16) can be simplified to

$$\begin{aligned}\Theta^{(1)}_{\ell m}(\vec{0}, \eta) &= \int_0^\eta d\eta' \int_0^\infty dx S_{\ell m}(x, \eta, \eta')\delta(x - \Delta\eta) \\ &= \int_0^\eta d\eta' \{g(\eta', \eta)[\theta_{0,\ell m}(\Delta\eta, \eta') + \Phi_{\ell m}(\Delta\eta, \eta') + V'_{b,\ell m}(\Delta\eta, \eta')] \\ &\quad + \gamma(\eta', \eta)(\Phi' + \Psi')_{\ell m}(\Delta\eta, \eta')\},\end{aligned} \tag{19}$$

which is just the harmonic decomposition of Eq. (5). Notice that in Eq. (5) $\hat{x} = \hat{l}$, so the gradient in the Doppler term can be written as a time derivative, which after integration by parts with the derivative of the delta function becomes the derivative of the baryon velocity in the expression above. This warm-up exercise is useful to check that all sources which contribute to temperature anisotropies at this level come from the light cone (its surface, in this case), which here appears explicitly as $\delta(x - \Delta\eta)$.

Another remarkable fact, which already shows up in this lowest-order approximation but which is true to all orders, is that the phases (ℓ, m) of the CMB observables are the same as the phases of the sources. The only conditions for this to hold are, first, that we keep to linear perturbation theory, and second, that the optical depth is a function of time only. We will see next that this holds true to higher orders in the total visibility γ.

B. γ^2 terms in position space

The expressions (11)–(13) are integral equations for the temperature and polarization momenta θ_ℓ and p_ℓ. We can iterate these equations and organize the series into powers of the total visibility, similarly to what is done for the Dyson series of quantum electrodynamics [26]—except that the fields in the integral equations for the CMB are coupled to a set of ordinary differential equations (the Einstein, continuity, and Euler equations for metric and matter perturbations.)

In the previous subsection we computed the first term of this series, which is of order γ^1 (since the source term is itself linear in γ). Consider now the next terms of this series, which are of order γ^2.

For polarization, we have that, to order γ^2, the only term which contributes is the temperature quadrupole to order γ^1. By substituting Eq. (12) into Eq. (13) and expressing the sources in terms of their spherical harmonic decompositions, like was done in the previous subsection, we obtain after some algebra:

$$\begin{aligned}P^{(2)}_{\ell m}(\vec{0}, \eta) = &-\frac{3}{2\pi}\sqrt{\frac{(\ell+2)!}{(\ell-2)!}}\int_0^\eta d\eta' g(\eta', \eta) \\ &\times \int_0^{\eta'} d\eta'' \int_0^\infty dx S_{\ell m}(x, \eta', \eta'') \\ &\times \int_0^\infty dk (kx)^2 j_\ell(kx)\frac{j_\ell(k\Delta\eta)}{(k\Delta\eta)^2} j_2(k\Delta\eta'),\end{aligned} \tag{20}$$

where $\Delta\eta' = \eta' - \eta''$. A simplified version of Eq. (20) was first written in this form by [38], for the case of the polarization from a galaxy cluster—where the visibility function after decoupling can be thought of being proportional to a Dirac δ-function, $g_c(\eta, \vec{x}) = \mu_c\delta(\vec{x} - \hat{n}\Delta\eta)$, where μ_c is a cluster's optical depth and $\hat{n}$ is the line of sight to the cluster.

Physically, this contribution to polarization corresponds to the photons that decoupled at some radius x and time η'', are scattered at time η', and then end up as a polarized beam at time η. The geometry is shown in Fig. 2. We will show now that the integral over k at the end of Eq. (20) has exactly that meaning: it vanishes unless the distances x, $\Delta\eta$, and $\Delta\eta'$ form a triangle, and such a triangle does not exist unless the sources are inside the PLC of the last scattering point, and the point of last scattering lies inside the PLC of the observation point. We will give a general expression for integrals such as this in Appendix A, but here is the result [28], which also defines our spacetime

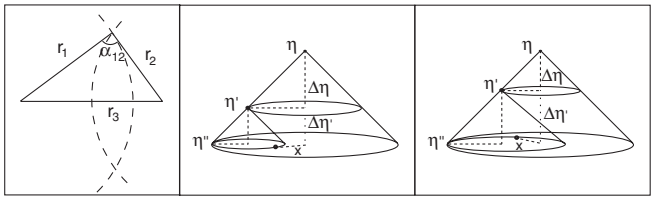

FIG. 2. Left panel: if the triangle of sides r_1, r_2, and r_3 exists, then the window function W_ℓ^3 is nonzero. Middle and right panels: spacetime diagrams for the scatterings, where time runs up, and space (radial coordinates) runs horizontally from the center to the sides. The diagrams show sources which decoupled at η'', then scatter off free electrons at time η', and end up contributing to the polarization $P_{\ell m}^{(2)}$ at time (η). The minimal and maximal values of x for which the sources can contribute to polarization are given by $x_{\rm min} = |\Delta\eta - \Delta\eta'|$ and $x_{\rm max} = \Delta\eta + \Delta\eta' = \eta - \eta''$.

window function W_ℓ^3:

$$W_\ell^3(r_1, r_2; r_3) = \frac{r_1^2}{r_2^2}\int_0^\infty dk j_\ell(kr_1) j_\ell(kr_2) j_2(kr_3) = \frac{\pi}{4}\frac{r_1^3}{r_2 r_3^3} P_\ell^{(-2)}(\cos\alpha_{12})\sin^2\alpha_{12}, \quad (21)$$

where

$$\cos\alpha_{12} = \frac{r_1^2 + r_2^2 - r_3^2}{2 r_1 r_2} \quad (22)$$

is the cosine of the angle between the sides r_1 and r_2 in the triangle of sides r_1, r_2, and r_3. The window function W_ℓ^3 is zero if that triangle does not exist, which means that it is nonzero only if the following set of conditions are satisfied:

$$r_1 \le r_2 + r_3, \qquad r_2 \le r_3 + r_1, \qquad r_3 \le r_1 + r_2, \quad (23)$$

or, equivalently, $|r_1 - r_2| \le r_3 \le r_1 + r_2$—see the left panel of Fig. 2. Notice how these triangular conditions mimic precisely the ones that appear in the addition of angular momentum eigenstates.

The window function (21) was first computed in Ref. [38]. We show plots for some of those window functions in the Appendix, Figs. 5–7.

Hence the momentum integral in Eq. (20) is $W_\ell^3(x, \Delta\eta; \Delta\eta')$, which means that it is a *spacetime window function* that vanishes unless the inequalities above are satisfied. What this result implies to our Eq. (20) is that a source at radius x and time η'' can only contribute to $P_{\ell m}^{(2)}(\eta)$ if $|\Delta\eta - \Delta\eta'| \le x \le \Delta\eta + \Delta\eta' = \eta - \eta''$. As the right panel of Fig. 2 shows, this spacetime window function limits the contributions of the sources to the PLCs of the last scatterings, and the scatterings themselves to the PLC of the observation point. Obviously, this means that the sources that contribute to $P_{\ell m}^{(2)}$ must also be inside the PLC of the observation point—which in this case is $\eta - \eta''$.

Let us summarize this result for the lowest-order contribution to polarization in position space:

$$P_{\ell m}^{(2)}(\vec{0}, \eta) = -\frac{3}{2\pi}\sqrt{\frac{(\ell+2)!}{(\ell-2)!}}\int_0^\eta d\eta' g(\eta', \eta)\int_0^{\eta'} d\eta'' \times \int_0^{\eta-\eta''} dx S_{\ell m}(x, \eta', \eta'') W_\ell^3(x, \Delta\eta; \Delta\eta') \quad (24)$$

Notice that, among other restrictions, the window function above cuts off the spatial integral at radius x at $\eta - \eta''$, which is where the PLC of the observation point lies at time η''.

In [38], Eq. (24) was used as the starting point to show how to invert the polarization data from galaxy clusters in order to reconstruct the three-dimensional map of the sources at the time of decoupling. That constitutes the solution (to lowest order in visibility) to a conjecture by Kamionkowski and Loeb about how to get around cosmic variance using cluster polarization [43].

Therefore, just as happened in the previous subsection with $\Theta_{\ell m}^{(1)}$, the integral over k in effect guarantees that the sources will only be taken into account if the scattering processes happen on the light cones. As before, the integral over x in Eq. (20) is cut off at $x_{\rm max} = \eta - \eta''$, eliminating sources which lie outside the PLC of the observation point $(\vec{0}, \eta)$. But now there is another feature: since $x_{\rm min} = |\Delta\eta - \Delta\eta'|$, sources which were too close to the observation point at time η'' also cannot contribute to the CMB at time η if last scattering happened at time η'—see the middle and right panels of Fig. 2. This additional constraint on the volume of the PLC which is integrated applies for times of last scattering (η') which are both close and far from the observation time η.

Before we turn to the order γ^3 terms, we write down the order γ^2 contribution to the temperature anisotropies, which comes from inserting $\theta_2^{(1)}$ into Eq. (11). After a calculation very similar to the one done above for polarization, we obtain that:

$$\Theta_{\ell m}^{(2)}(\vec{0}, \eta) = \frac{1}{4}\int_0^\eta d\eta' g(\eta', \eta)\int_0^{\eta'} d\eta'' \times \int_0^\infty dx S_{\ell m}(x, \eta', \eta'')\int_0^\infty dk (kx)^2 j_\ell(kx) \times \left[1 + 3\frac{\partial^2}{\partial(k\Delta\eta)^2}\right] j_\ell(k\Delta\eta) j_2(k\Delta\eta'). \quad (25)$$

The integral over k on the last line of the previous equation can be recast in terms of W_ℓ^3 if we use the recursion relations for the derivatives of spherical Bessel functions:

$$z^{\mp\ell}\frac{d}{dz}[z^{\pm\ell} j_\ell(z)] = \pm j_{\ell\mp1}(z). \quad (26)$$

The momentum integral then becomes:

$$(x\Delta\eta)^{-\ell-1}\frac{d}{dx}\frac{d}{d\Delta\eta}[x^{\ell-1}\Delta\eta^{\ell+3}W^3_{\ell+1}(x,\Delta\eta;\Delta\eta')] + 3\frac{\partial^2}{\partial\Delta\eta^2}\left[\frac{\Delta\eta^2}{x^2}W^3_\ell(x,\Delta\eta;\Delta\eta')\right],$$

which shows that, just as happened for polarization, the contribution of order γ^2 to the temperature is also modulated by the same spacetime window function.

C. γ^3 and higher-order terms in position space

The iteration process is trivial, but the higher order terms become lengthy. We present the result for the simplest γ^3 term that contributes to polarization:

$$\begin{aligned}P^{(3)}_{\ell m}(\vec{0},\eta) = &-\frac{27}{2\pi}\sqrt{\frac{(\ell+2)!}{(\ell-2)!}}\int_0^\eta d\eta' g(\eta',\eta)\\ &\times\int_0^{\eta'} d\eta'' g(\eta'',\eta')\\ &\times\int_0^{\eta''} d\eta'''\int_0^\infty dx S_{\ell m}(x,\eta'',\eta''')\\ &\times\int_0^\infty dk(kx)^2 j_\ell(kx)\frac{j_\ell(k\Delta\eta)}{(k\Delta\eta)^2}\\ &\times\frac{j_2(k\Delta\eta')}{(k\Delta\eta')^2}j_2(k\Delta\eta''),\end{aligned} \tag{27}$$

where $\Delta\eta'' = \eta'' - \eta'''$. We will show in Appendix A that the integral over k can be resolved into

$$\begin{aligned}W^4_\ell(r_1,r_2;r_3,r_4) &= \frac{r_1^2}{r_2^2 r_3^2}\int_0^\infty dk k^{-2} j_\ell(kr_1)j_\ell(kr_2)j_2(kr_3)\\ &\quad\times j_2(kr_4)\\ &= \frac{1}{2}\int d(\cos\alpha_{34})\frac{r_4^2}{r^2}P_2^{(-2)}\\ &\quad\times(\cos\alpha_{34})\sin^2\alpha_{34}\times\frac{\pi}{4}\frac{r_1^3}{r_2 r^3}P_\ell^{(-2)}\\ &\quad\times(\cos\alpha_{12})\sin^2\alpha_{12},\end{aligned} \tag{28}$$

where now r is defined as the common side of two triangles, of sides (r_1, r_2, r) and (r_3, r_4, r), such that $r^2 = r_1^2 + r_2^2 - 2r_1 r_2\cos\alpha_{12} = r_3^2 + r_4^2 - 2r_3 r_4\cos\alpha_{34}$—see Fig. 3. It is trivial to show that all the remaining terms of order γ^3 that contribute to the CMB temperature and polarization can be written in terms of the window function W^4_ℓ by using the recursion relations of spherical Bessel functions.

The window function vanishes unless all four sides can form a (flat) polygon, so inequalities similar to those found for W^3_ℓ apply here as well:

$$\begin{aligned}&r_1 \le r_2 + r_3 + r_4, \qquad r_2 \le r_3 + r_4 + r_1,\\ &r_3 \le r_4 + r_1 + r_2, \qquad r_4 \le r_1 + r_2 + r_3.\end{aligned} \tag{29}$$

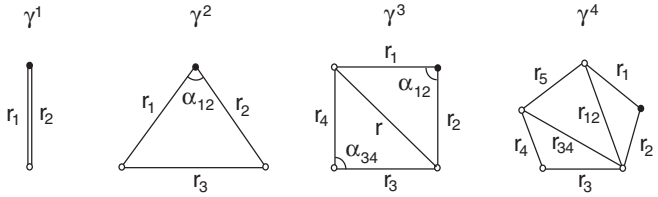

FIG. 3. Diagrammatic representation of the series in the visibility. In all diagrams, the filled dot corresponds to the point and time of observation of the CMB temperature and polarization. The γ^1 term (the two lines beginning and ending at the same points) corresponds to a window function $\delta(r_1 - r_2)$. The γ^2 and γ^3 terms (respectively the triangle and 4-side polygon) correspond to the window functions W^3_ℓ of Eq. (21) and W^4_ℓ of Eq. (28). For all diagrams the window functions vanish unless the sides are such that the polygon can be closed. The main physical implication is that sources (which by default are located at r_1 with respect to the observation point) outside the PLCs of the last scatterings do not contribute to the CMB. In particular, sources outside the PLC of the point of observation are thrown out of the integration of the physical observables. See the Appendix for a full discussion of these geometrical properties.

Again, these are exactly the same conditions that appear in the addition of three angular momentum eigenstates.

The conditions stated above imply once again that the sources can only contribute to the observable at time η if each successive PLC lies inside the previous PLC, all the way from the observation point back to the sources. The constraints on the positions of the sources are now more complicated than the case of two scatterings, but the diagrams in Fig. 4 show which values of x (measured from the origin, at the middle of the bases of the cones) are allowed by the window functions. In three spatial dimensions, these ranges of radii correspond to concentric spherical shells—

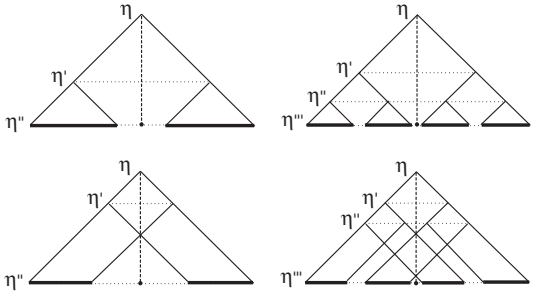

FIG. 4. Structure of the successive PLCs for two (left diagrams) and three (right diagrams) scatterings. The values of x for which the window functions $W^3_\ell(x,\eta;\eta')$ and $W^4_\ell(x,\eta;\eta',\eta'')$ are nonzero are indicated as the thick lines at the bases of the cones. Here the radius x should be measured from the origin of the spatial coordinates, which in these spacetime diagrams lie along the dashed lines. Notice that the region in the vicinity of the PLC of the observation point (the outermost PLC) always contributes to the integral, the origin is always excluded, and intermediate regions may or may not contribute to the CMB observables.

in the case of two scatterings, there is one spherical shell; in the case of three scatterings, two spherical shells; and so on. The outermost spherical shell always includes the edge of the PLC of the observation point.

It is easy to recover W^3_ℓ from W^4_ℓ by taking $r_3 \to 0$. In fact, we can also recover the orthogonality condition for the spherical Bessel functions, Eq. (18), from W^3_ℓ by taking $r_3 \to 0$. This can be made by noticing that, in W^3_ℓ the limit $r_3 \to 0$ leads to $r_2 = r_1$, and in W^4_ℓ the limit $r_3 \to 0$ leads to $r_4 = r$. Then, using the expansion of the Bessel functions for small arguments, $j_2(z) \approx z^2/15 + \mathcal{O}(z^4)$, we obtain that

$$\lim_{r_3\to 0} W^3_\ell(r_1, r_2; r_3) = \frac{r_3^2}{15} \times \frac{\pi}{2} r_1^{-2} \delta(r_1 - r_2), \tag{30}$$

$$\lim_{r_3\to 0} W^4_\ell(r_1, r_2; r_3, r_4) = \tfrac{1}{15} \times W^3_\ell(r_1, r_2; r_4). \tag{31}$$

The first identity just shows that the PLC delta function is the spacetime window function for two scatterings (order γ^1.) The second identity can also be verified by noticing that in the $r_3 \to 0$ limit, $\cos\alpha_{34}$ is unconstrained, so we can integrate out the dependence on that angle, which gives a factor of $2/15$.

The procedures outlined above can be extended once again to the next order in the visibility, γ^4. The geometrical interpretation is given by the right-most diagram in Fig. 3. Again, we see the role played by the spacetime window functions, of regulating the volume of the PLC in each scattering so that the information from the sources is propagated causally all the way to the observer. Notice also that by taking $r_3 \to 0$ we recover W^4_ℓ—in fact, all the spacetime window functions obey the relation

$$\lim_{r_3\to 0} W^n_\ell(r_1, r_2; r_3, \ldots, r_n) = \tfrac{1}{15} W^{n-1}_\ell(r_1, r_2; r_4, \ldots, r_n)$$

D. Interpretation of the series in γ

In this Section we have shown, first, that the contribution of order γ^1 from sources at positions x and times of last scattering η' to the temperature which is observed at time η is modulated by a delta-function, $\delta(x - \Delta\eta)$—and this is nothing but the surface of the PLC of the observation point, $x = \Delta\eta = \eta - \eta'$. Then we showed that the contributions of order γ^2 to temperature and polarization are modulated by the spacetime window function $W^3_\ell(x, \Delta\eta; \Delta\eta')$, where now $\Delta\eta$ denotes the interval between observation and the last scattering, and $\Delta\eta'$ denotes the interval between that last scattering and the second-to-last scattering. We presented the simplest contribution of order γ^3, which sums over sources modulated by the window function W^4_ℓ, and indicated how the order γ^4 term is also modulated by a window function W^5_ℓ. Notice that we have been labeling each term of the series in terms of γ, which in this notation stands both for the *total* visibility $\gamma = e^{-\mu}$ and for the visibility *function* $g = d\gamma/d\eta$. However, even though the total visibility is always smaller than unity, the visibility function is highly peaked at the time of recombination and during reionization, so it would be incorrect to characterize our series over visibility as a perturbative series—it is rather more like an asymptotic series.

The series over visibility has the diagrammatic representation shown in Fig. 3. Perhaps it is not so surprising that the spherical Bessel functions play a key role in regulating the volume inside the PLC, since they are associated with the matrix elements of E_3—the Euclidean group in three dimensions [44]. E_3 is a noncompact group consisting of the set of transformations under which distances are invariant, which may explain why the spherical Bessel functions modulate the (invariant) distances on each equal-time hypersurface.

Another check on our results is the fact that all the window functions are real. Since the sources $S(\vec{x}, \eta, \eta')$ are themselves real, this means, in particular, that $P^*_{\ell m} = (-1)^m P_{\ell,-m}$—i.e., the polarization that is generated from scalar perturbations is made up purely of E-modes. If we had included gravity waves or lensing, these window functions would have acquired an imaginary piece as well, which would have "magnetic" (instead of "electric") parity and therefore generate B-modes.

The spacetime window functions to any order in γ vanish unless each scattering lies in the PLC of the following scattering, all the way from the sources to the observation point. The order γ^N contributions to CMB observables hold the information from the Nth last scatterings, and are modulated by the window function $W^{N+1}_\ell(x, \Delta\eta; \Delta\eta_1, \ldots, \Delta\eta_{N-1})$. In terms of the diagrams of Fig. 3, there are always two spherical Bessel functions of order ℓ, corresponding to the source (x) and the last scattering before observation ($\Delta\eta$), and $N-1$ spherical Bessel functions of order 2, corresponding to the $N-1$ intermediate scatterings for which the quadrupoles of the temperature and polarization served as sources in the iterations of the line-of-sight integrals. The computation of these spacetime window functions, as well as the restrictions they impose on the sources that can contribute to the CMB (in particular the fact that they all vanish outside the PLC of the observation point) are shown in Appendix A.

Therefore, in position space the line-of-sight integral equations have a simple interpretation in terms of successive Thomson scatterings happening along the successive PLCs. These expressions should still be coupled to the Einstein, continuity, and Euler equations through the temperature dipole and quadrupole, but those are local equations so their causal structure is trivial (nevertheless, the Green's function in position space for the cosmological matter and metric perturbations can also reveal very interesting features [34,35].)

Going back to the hierarchy of Boltzmann equations, which are obtained directly from the line-of sight integrals

in Fourier space, there is one full hierarchy which holds separately for each mode $\{k, \ell, m\}$. Hence, what we have shown is an explicit demonstration that the line-of-sight formalism can also be seen as the solution to an initial values problem, where the initial conditions only need to be specified inside the PLC of the observer, at some initial time when the visibility was small enough that the series converges quickly. In other words: we have explicitly shown that the line-of-sight integrals in Fourier space are essentially the Fourier transform of a retarded Green's function for the CMB observables. These retarded Green function for anisotropies in position space are expressed at each order in the series over visibility through spacetime window functions, which are ultimately the objects responsible for enforcing causality and regulating which inhomogeneities are able to affect anisotropies, and how.

The results of this section have an interesting connection with schemes to simulate constrained maps of CMB temperature and polarization [29–33]. These simulations are extremely important to predict the types and levels of non-Gaussianity in the CMB which are generated at the very early Universe, since distinct inflationary models can be differentiated on that basis [45]. In those simulations, the temperature and polarization transfer functions, which transform the inhomogeneities (the sources) into anisotropies, are computed numerically assuming some visibility function. Moreover, some approximations are typically made, such as considering only the curvature perturbation in the source term. Our expressions, on the other hand, are exact and analytical, but it is not immediately clear how (or if) they could be used to facilitate a simulation. However, our results show that the transfer functions of [29,30] are made up of invariant (or geometrical) pieces which can be factored from the purely time-dependent visibility function. These invariant parts are given by our spacetime window functions, which do not depend on the cosmological scenario or on the history of recombination. The transfer functions relevant for the simulations can, therefore, be obtained by integrating our spacetime window functions over time with some visibility function.

IV. CMB WITH THE FOURIER-BESSEL EXPANSION

We have seen that the line-of-sight integrals for the CMB temperature and polarization, when framed in position space, lead to spacetime window functions that constrain the positions of the sources $S(x)$ that are eventually integrated over. These constraints, valid at each order in the visibility, imply, in particular, that the sources must all lie inside the PLC of the observer that measures the CMB. But this is not the only constraint that is relevant for this problem.

The physics of recombination is such that the visibility is exponentially small for $z \gg 10^3$. Since all the terms of the series over visibility are linear on the sources, the fact that they are always multiplied by powers of the visibility implies that the sources which are relevant in the line-of-sight integrals are those that lie inside the PLC of the observer at some time late enough that the visibility is nonvanishing. So, the sources which are actually summed into the CMB anisotropies are not simply the sources in the PLC of the observer, but the sources in the PLC of the observer at times such that the visibility is not totally negligible. Since for a typical flat ΛCDM cosmology the lookback distance from today to those early times saturates near $R \sim 5H_0^{-1}$ for $z \gg 10^3$, it makes little difference whether we choose that initial instant (when $\gamma \to 0$ and $g \to 0$) to be $z = 10^4$, 10^5, or 10^{10}.

This means that the integration of the sources is not simply limited to the PLC of the observer, as implied by the window functions W_ℓ^N, but that the relevant spacetime volume is that of the PLC, cut off at some initial time η_i such that $\gamma(\eta, \eta_i)$ and $g(\eta, \eta_i)$ are sufficiently small. Since the unperturbed spacetime is symmetric around the source, there is in effect a maximal radius away from the observer, $R = \eta - \eta_i$, such that outside that radius, the sources are effectively zero by virtue of the powers of γ that multiply them at each order in the series. Notice that we could even choose R to be bigger than this lookback time, but that would unnecessarily include sources which are eventually discarded in the integration of the physical observables.

Hence, we can fix some boundary R and set all fields to zero at that boundary and beyond: the result of solving the initial values problem through the line-of-sight integrals will be exactly the same, order by order in the series over the visibility.

If that is the case, then we should ask what would be the best way to represent the sources, considering that they are zero at and above some radius R from the origin. The appropriate expansion in that case is clearly the Fourier-Bessel series [28], for which the fields are expanded in spherical harmonics and spherical Bessel functions, but instead of the continuum of momenta that appears in Fourier space, Eq. (15), the modes are discretized: they are given by the roots of the spherical Bessel functions. A function that obeys Dirichlet boundary conditions at $r = R$ is expanded as

$$f(\vec{x}) = \sum_{\ell m} f_{\ell m}(x) Y_{\ell m}(\hat{x}) = \sum_{\ell m} \sum_{i=1}^{\infty} f_{i\ell m} j_\ell(k_{i\ell} x) Y_{\ell m}(\hat{x}), \tag{32}$$

where the last sum is over the ith root of j_ℓ, so that for all i's the Bessel functions vanish at the boundary, $j_\ell(k_{i\ell} R) = 0$. The coefficients $f_{i\ell m}$ can be obtained by using the orthogonality relation of the Fourier-Bessel basis:

$$\int_0^1 dz z^2 j_\ell(q_{i\ell} z) j_\ell(q_{j\ell} z) = \frac{1}{2}[j_{\ell+1}(q_{i\ell})]^2 \delta_{ij}, \tag{33}$$

where $q_{i\ell}$ is the ith root of $j_\ell(z)$. This expression leads immediately to

$$f_{i\ell m} = \frac{2R^{-3}}{j^2_{\ell+1}(k_{i\ell}R)} \int_0^R dx x^2 j_\ell(k_{i\ell}x) f_{\ell m}(x), \tag{34}$$

where $k_{i\ell} = q_{i\ell}/R$.

The most important feature of the Fourier-Bessel series is that its basis functions, like the plane waves of the Fourier expansion, are eigenvectors of the Laplacian operator in flat space, $\nabla^2 j_\ell(k_{i\ell}x)Y_{\ell m}(\hat{x}) = -k^2_{i\ell} j_\ell(k_{i\ell}x) \times Y_{\ell m}(\hat{x})$. This means that the Einstein, continuity and Euler equations for matter are exactly the same as in the usual Fourier expansion—except that the momenta $k_{i\ell}$ are now discretized. Moreover, the lowest eigenmode of the Fourier-Bessel series that can contribute for a given multipole ℓ is $k_{1\ell} \sim \ell/R$. If the spatial sections are curved, the only difference is that the radial functions are the so-called ultraspherical Bessel functions—see, e.g., [24]—however, the fact that the radial and angular modes can be separated in the linear theory remains an exact statement, and the fact that the momenta are discretized in a Fourier-Bessel type of expansion also remains true.

Notice that there is nothing fundamental about the radius R of the spherical box inside which we define initial conditions for the CMB observables: we could have chosen to cut off the light cone at an earlier time, for instance, which would make R larger. This would mean that the modes would be shifted by a factor $k_{i\ell} \to R_{\rm old}/R_{\rm new} k_{i\ell}$—however, the hierarchy between the different modes would remain exactly the same, i.e., the fractions $k_{i\ell}/k_{i'\ell'} = q_{i\ell}/q_{i'\ell'}$ are invariant under a scaling of R. This tells us that it is this hierarchy between the discretized momenta that is responsible for the optimization of the information that eventually gets transferred to the CMB.

Finally, we could have also chosen Neumann boundary conditions for the functions expanded inside that spherical box. This choice would lead to a different set of modes $\bar{q}_{i\ell}$, corresponding to the roots of the equations $j'_\ell(q_{i\ell}) = 0$. Still there is a minimum mode, and a tower of discretized modes above that minimum. In practical applications it may turn out to be convenient to use either one of these sets of modes—or perhaps even both sets.

A. Fourier-Bessel modes of CMB observables

Now we can go back to the CMB and translate the equations and methods presented in the previous Sections to the Fourier-Bessel basis. The most important difference between the two expansions can be grasped by comparing Eqs. (15), (32), and (34). Basically, when going from the Fourier basis to the Fourier-Bessel basis, the angular dependence is still expressed in terms of spherical harmonics, but the radial coordinate is expressed by a sum, not an integral:

$$\sqrt{\frac{2}{\pi}} i^\ell \int_0^\infty dk k^2 \to R^{-3} \sum_i, \tag{35}$$

which just tells us how to go from the continuum of momenta appropriate for fields in $\mathbb{R}^3$ to the discrete tower of momenta $k_{i\ell}$ that encapsulates all the information for fields limited to the finite volume inside a sphere of radius R.

In particular, this means that now the CMB temperature and polarization are given in terms of the momenta not by Eqs. (9) and (10), but by

$$\Theta_{\ell m}(\eta) = \sum_i \Theta_{i\ell m}(\eta), \tag{36}$$

$$P_{\ell m}(\eta) = \sum_i P_{i\ell m}(\eta). \tag{37}$$

In these sums $\Theta_{i\ell m} \equiv \theta_{\ell, i\ell m}$ and $P_{i\ell m} \equiv p_{\ell, i\ell m}$ are given by the solutions of integral equations analogous to Eqs. (11)–(13), which for each multipole L and for each mode $\{i\ell m\}$ read

$$\theta_{L,i\ell m}(\eta) = \theta^{(1)}_{L,i\ell m}(\eta) + \frac{1}{4}\int_0^\eta d\eta' g(\eta', \eta)[\theta_{2,i\ell m}(\eta') - \sqrt{6} p_{2,i\ell m}(\eta')]\left[1 + 3\frac{\partial^2}{\partial(k_{i\ell}\Delta\eta)^2}\right] j_L(k_{i\ell}\Delta\eta), \tag{38}$$

$$\theta^{(1)}_{L,i\ell m}(\eta) = \int_0^\eta d\eta' S_{i\ell m}(\eta, \eta') j_L(k_{i\ell}\Delta\eta), \tag{39}$$

$$p_{L,i\ell m}(\eta) = -\frac{3}{4}\sqrt{\frac{(\ell+2)!}{(\ell-2)!}} \int_0^\eta d\eta' g(\eta', \eta)[\theta_{2,i\ell m}(\eta') - \sqrt{6} p_{2,i\ell m}(\eta')] \frac{j_L(k_{i\ell}\Delta\eta)}{(k_{i\ell}\Delta\eta)^2}, \tag{40}$$

and where the sources in Eq. (39), which were defined in Eq. (17), have been expanded in the Fourier-Bessel basis as well. Notice that only the generalized modes $\{L; i, \ell, m\}$ with $L \leq 2$ really need to be calculated from the integral equations (or, equivalently, from the associated Boltzmann equations), since all the higher modes ($L \geq 3$) can be computed from the former, and only the pieces $L = \ell$ actually get summed into the CMB observables, Eqs. (36) and (37). This is just a restatement of the fact that the sources of anisotropies are the matter and metric inhomogeneities, plus the dipole and quadrupole of temperature and polarization—which, again, underpins the vast superiority of the line-of-sight formalism compared to the full hierarchy of Boltzmann equations.

An important check of consistency is to reobtain the temperature and polarization anisotropies in position space that were derived in Sec. III. To first order in γ, the temperature anisotropies are given by

$$\Theta^{(1)}_{\ell m}(\eta) = \sum_i \theta^{(1)}_{\ell, i\ell m} = \int_0^\eta d\eta' \int_0^R dx x^2 \sum_i \frac{2R^{-3}}{j^2_{\ell+1}(k_{i\ell}R)} j_\ell(k_{i\ell}x) \times S_{\ell m}(x, \eta, \eta') j_\ell(k_{i\ell}\Delta\eta), \quad (41)$$

where the source term $S_{\ell m}(x, \eta, \eta')$ was defined in Eq. (17). But now the infinite sum in Eq. (41) can be resolved through the use of the orthogonality of the Fourier-Bessel basis in target space (actually, this is a completeness relation—see [28], Chap. XVIII), which is just the Fourier-Bessel counterpart of Eq. (18):

$$\sum_{i=1}^\infty \frac{j_\ell(k_{i\ell}r_1) j_\ell(k_{i\ell}r_2)}{j^2_{\ell+1}(k_{i\ell}R)} = \frac{1}{2} R^3 r_1^{-2} \delta(r_1 - r_2). \quad (42)$$

This identity leads then automatically to Eq. (19), which shows that to order γ^1 the Fourier and Fourier-Bessel descriptions are identical.

To order γ^2 it is less obvious that one obtains the same anisotropies as related to the position-space fields, but it is true nevertheless. To see that, take the simplest term—the contribution to polarization that comes from the order γ^1 quadrupole:

$$P^{(2)}_{\ell m}(\eta) = \sum_i p_{\ell, i\ell m} = -\frac{3}{4}\sqrt{\frac{(\ell+2)!}{(\ell-2)!}} \int_0^\eta d\eta' g(\eta', \eta) \times \int_0^{\eta'} d\eta'' \int_0^\infty dx x^2 \sum_i \frac{2R^{-3}}{j^2_{\ell+1}(k_{i\ell}R)} S_{\ell m}(x, \eta', \eta'') \times j_\ell(k_{i\ell}x) \frac{j_\ell(k_{i\ell}\Delta\eta)}{(k_{i\ell}\Delta\eta)^2} j_2(k_{i\ell}\Delta\eta'). \quad (43)$$

Notice that now, making $r_1 = x$, $r_2 = \Delta\eta$ and $r_3 = \Delta\eta'$ we have on the right-hand side a spacetime window function given by

$$\tilde{W}^{\,3}_\ell(r_1, r_2; r_3) = \pi R^{-3} \frac{r_1^2}{r_2^2} \sum_{i=1}^\infty \frac{1}{k^2_{i\ell}} \times \frac{j_\ell(k_{i\ell}r_1) j_\ell(k_{i\ell}r_2) j_2(k_{i\ell}r_3)}{j^2_{\ell+1}(k_{i\ell}R)}. \quad (44)$$

Although we have not been able to prove mathematically that this Fourier-Bessel window function is identical to the Fourier window function of Eq. (21), we have checked numerically that they are identical—including the factor of π which relates the phase spaces of the two basis functions. Hence, the lowest-order contribution to CMB polarization that results from using the Fourier-Bessel representation is again given, precisely, by Eq. (24).

In fact, we can prove (see the Appendix) not only that the two window functions W^3_ℓ and $\tilde{W}^3_\ell$ are equal, but that *all* the window functions derived in Sec. III are identical to the window functions that arise in the Fourier-Bessel expansion, if a certain generalization of the orthogonality relation, Eq. (42), is valid:

$$\sum_{i=1}^\infty \frac{j_{\ell'}(k_{i\ell}r_1) j_{\ell'}(k_{i\ell}r_2)}{j^2_{\ell+1}(k_{i\ell}R)} = \frac{1}{2} R^3 r_1^{-2} \delta(r_1 - r_2). \quad (45)$$

We have checked numerically that this relation seems to hold true for a range of ℓ and ℓ', and for any arguments $0 \leq r_{1,2} < 1$, but as far as we know this has not been proven anywhere in the literature about Bessel functions—even though it clearly is a fundamental tool for relating quantities in the Fourier and in the Fourier-Bessel expansions.

We have also checked that the integral equations (38)–(40) lead to the usual hierarchy of Boltzmann equations [16,23,25], where now there is one full independent hierarchy for each mode $\{i\ell m\}$. It is curious that, while in the usual Fourier analysis what generates the hierarchy of Boltzmann equations are the recursion relations of the Legendre polynomials in the angular dependence $\hat{k}\cdot\hat{l}$, in our case the generators of the hierarchy are the recursion relations of the radial modes—the spherical Bessel functions. Since the two special functions are intimately related by Rayleigh's expansion of the plane wave (which is ultimately what regulates the line-of-sight integrals), it is indeed natural that both bases could be used to generate that hierarchy.

The crucial difference between the Fourier-Bessel series and the usual Fourier analysis lies in the discrete momenta $k_{i\ell}$ that can contribute to the observables $\Theta_{\ell m}$ and $P_{\ell m}$ in the Fourier-Bessel expansion. Critically, in this discretized series the first mode to contribute at each multipole is $k_{1\ell} \sim \ell/R$. Another feature is that the total number of modes which one needs to compute to obtain anisotropies up to some $\ell_{\max}$ is $N_{\max} \sim \ell^2_{\max}/9$ (for $\ell_{\max} \gg 10$).

There is, however, an apparent drawback of the Fourier-Bessel basis: although it clearly is a superior method to solve our sort of initial values problem when compared to the Fourier basis, when the underlying spatial fields are Gaussian the coefficients of the Fourier-Bessel series do not obey simple statistics like those of the Fourier modes. We will now turn to these issues.

B. Statistics and power spectra in the Fourier-Bessel basis

Take a Gaussian field $f(\vec{x})$ in $\mathbb{R}^3$, which is expanded into spherical harmonics in position and in Fourier space as in Eqs. (14). If homogeneity and isotropy are unbroken, the two-point correlation functions in position and in Fourier space can be expressed in terms of the radial functions as

$$\langle f_{\ell m}(r) f^*_{\ell' m'}(r') \rangle = \delta_{\ell\ell'}\delta_{mm'}\xi^f_\ell(r, r'), \quad (46)$$

$$\langle f_{\ell m}(k) f^*_{\ell' m'}(k') \rangle = \delta_{\ell\ell'}\delta_{mm'} k^{-2} P_f(k) \delta(k - k'). \quad (47)$$

Here the advantage of Fourier space becomes evident:

translational invariance implies that the covariance matrix of the Fourier modes is completely diagonal. The relationships between the position-space two-point correlation function and the power spectrum are given by

$$\xi^f_\ell(r, r') = \frac{2}{\pi}\int_0^\infty dk k^2 j_\ell(kr) j_\ell(kr') P_f(k), \tag{48}$$

and, conversely, by

$$P_f(k) = \int_0^\infty dr r^2 \frac{j_\ell(kr)}{j_\ell(kr')}\xi^f_\ell(r, r'). \tag{49}$$

From the identity above it is also evident that the two-point correlation function has a lot of redundant information, since many different traces of it can lead to the power spectrum. If the field f is Gaussian, these correlation functions are the only nontrivial statistical momenta of that field's distribution function.

We want to obtain the corresponding relations for the modes of the Fourier-Bessel series. This can be easily achieved by taking fields $f(\vec{x})$ in $\mathbb{R}^3$ and passing them through a radial window function $W(r)$, such that $W(r \geq R) = 0$—e.g., the top hat window function:

$$W^{TH}(r) = \theta(R - r), \qquad W^{TH}(k) = \sqrt{\frac{2}{\pi}}\frac{R^3}{kR} j_1(kR), \tag{50}$$

where $\theta(x)$ is the step (Heaviside) function. In this way, the filtered functions will obey the boundary conditions, $\tilde{f}(R) = W(R) f(R) = 0$.

In Fourier space, the effect of a window function is to couple the different modes

$$\tilde{f}(\vec{k}) = \int \frac{d^3q}{(2\pi)^{3/2}} W(\vec{k} - \vec{q}) f(\vec{q}). \tag{51}$$

Hence, the Fourier transform of the filtered function acquires nondiagonal correlations k-space

$$\langle \tilde{f}(\vec{k})\tilde{f}^*(\vec{k}')\rangle = \int \frac{d^3q}{(2\pi)^3} W(\vec{k} - \vec{q}) W(\vec{k}' - \vec{q}) P_f(q). \tag{52}$$

For a purely radial window function $W(r)$, we obtain with the help of Eqs. (15) that the spherical harmonic components of the filtered function are

$$\tilde{f}_{\ell m}(k) = \int dq q^2 f_{\ell m}(q) W_\ell(k, q), \tag{53}$$

where $W_\ell(k, q)$ is the (symmetric) mode-coupling kernel of the radial window function

$$W_\ell(k, q) = \frac{2}{\pi}\int_0^\infty dr r^2 W(r) j_\ell(kr) j_\ell(qr). \tag{54}$$

Hence, it is clear that if $W(r) \to 1$ then $W_\ell(k, q) \to q^{-2}\delta(k - q)$ and we recover the Fourier modes of the $\mathbb{R}^3$ field. For a generic radial window function, however, there will be mixing of modes, and the covariance matrix will be nondiagonal. The filtered spectrum is then related to the physical power spectrum through

$$\langle \tilde{f}_{\ell m}(k)\tilde{f}^*_{\ell m}(k')\rangle = \int_0^\infty dq q^2 W_\ell(k, q) W_\ell(k', q) P_f(q). \tag{55}$$

In particular, for the Fourier-Bessel modes, which are related to the (filtered) spherical modes in Fourier space by $f_{i\ell m} = \sqrt{2\pi} i^\ell j^{-2}_{\ell+1}(k_{i\ell}R)\tilde{f}_{\ell m}(k_{i\ell})$, this last identity implies that

$$\begin{aligned}
\langle f_{i\ell m} f^*_{j\ell m}\rangle &= \frac{2\pi R^{-6}}{j^2_{\ell+1}(k_{i\ell}R) j^2_{\ell+1}(k_{j\ell}R)}\int_0^\infty dq q^2 W_\ell(k_{i\ell}, q) W_\ell(k_{j\ell}, q) P_f(q) \\
&= \int_0^R dr r^2 \frac{2R^{-3} j_\ell(k_{i\ell}r)}{j^2_{\ell+1}(k_{i\ell}R)}\int_0^R dr' r'^2 \frac{2R^{-3} j_\ell(k_{j\ell}r')}{j^2_{\ell+1}(k_{j\ell}R)} \times \frac{2}{\pi}\int_0^\infty dq q^2 P_f(q) j_\ell(qr) j_\ell(qr') \\
&= \int_0^R dr r^2 \frac{2R^{-3} j_\ell(k_{i\ell}r)}{j^2_{\ell+1}(k_{i\ell}R)}\int_0^R dr' r'^2 \frac{2R^{-3} j_\ell(k_{j\ell}r')}{j^2_{\ell+1}(k_{j\ell}R)}\xi^f_\ell(r, r'),
\end{aligned} \tag{56}$$

where we have used the top hat window function from the first to the second line. These expressions show how to compute the covariance of the Fourier-Bessel modes from either the power spectrum or from the two-point correlation function in position space. It is also useful to obtain the equivalent of Eq. (48) in the Fourier-Bessel representation. By the completeness relation, Eq. (42), it is easy to see that

$$\begin{aligned}
&\sum_i\sum_j j_\ell(k_{i\ell}r) j_\ell(k_{j\ell}r')\langle f_{i\ell m} f^*_{j\ell m}\rangle \\
&\quad = \theta(R - r)\theta(R - r')\xi^f_\ell(r, r'),
\end{aligned} \tag{57}$$

where $\theta(r)$ is the step (Heaviside) function.

The two-point correlation function (as opposed to the Fourier spectrum) is more directly related to the physical observables, since it remains invariant as long as we keep within the causally accessible region (i.e., $r \leq R$ and $r' \leq R$.) However, Eq. (56) also tells us that the two-point function of the Fourier-Bessel modes has nondiagonal terms (albeit only in k-space.) This does not pose a problem, because the spectrum is not really an observable: it can only be estimated (with exactly the same tools and assumptions as usual) from observables such as the temperature and polarization maps, as well as their derived products such as the angular power spectra. And since we saw in the previous section that the observables retain

exactly the same relations to the sources of anisotropies as they do in the usual Fourier expansion in $\mathbb{R}^3$, we conclude that the Fourier-Bessel expansion fulfills all the requirements to faithfully express the physics of the CMB.

C. Angular power spectra

Most of the useful cosmological information that we get from the CMB comes from the angular power spectra, because of their simple relationship with the Fourier power spectrum. For a function $f(\vec{x})$, the angular spectrum at radius r can be defined from Eq. (46), as $C_\ell^f(r) = \xi_\ell^f(r, r)$. Below we show that in the Fourier-Bessel expansion the angular power spectra assume exactly the same values as they would if we did not assume that the space was limited to the sphere $r \leq R$.

The argument is simplest for the temperature anisotropies to order γ^1, and generalizes in a trivial manner to the higher-order terms. The angular power spectrum for temperature in the Fourier-Bessel case reads

$$\langle \Theta_{\ell m}^{(1)} \Theta_{\ell' m'}^{(1)*} \rangle = \left\langle \sum_i \Theta_{i\ell m}^{(1)} \sum_{i'} \Theta_{i'\ell' m'}^{(1)*} \right\rangle = C_\ell^{TT(1)}(\eta) \delta_{\ell\ell'} \delta_{mm'}. \tag{58}$$

Using the orthogonality conditions of the Fourier-Bessel basis in target space, Eq. (42), we obtain

$$C_\ell^{TT(1)}(\eta) = \int^\eta d\eta_1' \int^\eta d\eta_2' \langle S_{\ell m}(x = \Delta\eta_1, \eta_1') \times S_{\ell m}^*(x = \Delta\eta_2, \eta_2') \rangle = \langle \bar{S}_{\ell m} \bar{S}_{\ell m}^* \rangle_{\mathrm{PLC}}. \tag{59}$$

But this is exactly the usual result: to lowest order, the temperature angular power spectrum is given by the average over the PLC of the (angular) two-point angular correlation function of the Sachs-Wolfe, Doppler, and integrated Sachs-Wolfe source terms, properly weighted by the visibility. For the γ^2 and higher-order terms, the procedure is precisely the same and leads back to the same relation between the angular power spectra and the sources as happened in position space, where the spacetime window functions regulate which sources contribute to the anisotropies in the space and time integrals. Hence, we have shown that not only the observables (the temperature anisotropies), but also that the statistics of the angular power spectra in the Fourier-Bessel expansion are identical to the usual case of the Fourier expansion.

D. Fourier *v.* Fourier-Bessel

The identity between the spacetime window functions at all orders in γ implies that the source and the observables (the temperature and polarization maps, or equivalently their spherical harmonic components $\Theta_{\ell m}$ and $P_{\ell m}$) are related in exactly the same way in the Fourier-Bessel basis and in the Fourier basis. The statistics of the angular power spectra, therefore, are also related to the statistics of the underlying matter and metric fields in precisely the same way in the two representations.

Hence, the Fourier-Bessel basis is, in some respects, completely equivalent to the Fourier basis: it represents the same physics and it expresses the same observables as its Fourier counterparts—it even has the same statistics. However, in at least one respect the Fourier-Bessel basis is superior to the Fourier basis: it has a precise prescription for the discretized tower of modes that contribute for the observables at each multipole. These modes take into account exactly the relevant pieces of information from the sources, the ones that propagate from the initial value surface to the physical observables—no more, no less. And the statistics of the power spectra, as we have demonstrated above, is related in precisely the same way to the statistics of the (presumably Gaussian) matter fields, just as happens in the usual analysis in Fourier space.

Finally, as an initial-value formulation the Fourier-Bessel expansion is vastly superior to the Fourier representation because it does not waste any resources keeping track of irrelevant variables such as super-Hubble modes or modes which trace out of the observable. All the information is encoded in a discrete series of momenta, and we do not have to guess how to subdivide the Fourier space in sufficiently small pieces in order to sample the observables we want to compute—the Fourier-Bessel modes already provide the unique, optimal choice.

V. CONCLUSIONS

In this paper we have shown how causality constraints in position space regulate which sources of anisotropies (the matter and metric perturbations) can contribute to the CMB. This causal structure is manifested order by order in a series of terms corresponding to the number of interactions that photons experienced over the past light cone of the observer—or, equivalently, a power series on the visibility $\gamma = e^{-\mu}$.

When expressed in position space, the line-of-sight integrals acquire an intuitive interpretation in terms of scatterings over the light cones of the successive scatterings, all the way from the sources to the point and time of observation. In particular, we find that, in position space, only the sources of anisotropy that are inside our past light cone are taken into account. This statement is exact to all orders—as it should be, since the causal nature of the propagation of photons is the key ingredient in the line-of-sight integrals from which we started. An interesting question which we did not have time to address is at what number of scatterings prior to free streaming we can cut off this series so that the error in the temperature distribution is, say, of order 1%.

At each order in the power series on the visibility, the sources are weighted by spacetime window functions. These window functions can be complicated for a high number of scatterings, but they all obey a very simple rule:

they vanish identically unless some extremely simple sets of inequalities are satisfied. These inequalities are identical to the triangle conditions that appear when adding angular momentum eigenstates, and have a simple geometrical interpretation: if the position of the source and the radii of the light cones of the interactions cannot form a flat polygon, the spacetime window functions vanish.

One of the implications of these causality constraints is that, whatever the properties of the Universe outside a limiting radius R, the source fields do not propagate to the CMB observables—and the line-of-sight integrals both in Fourier space and in the Fourier-Bessel expansion retain this property. In practice, this means that we can use the Fourier-Bessel framework to compute the CMB—even though it puts the Universe in a "spherical box," and discards all the information outside of that box.

In the Fourier-Bessel basis, the fields are decomposed in spherical harmonics and a series of discrete eingenmodes $k_{i\ell}$ (as opposed to the continous modes of Fourier space.) The first eigenmode for each multipole ℓ is $k_{1\ell} \sim \ell/R$. CMB observables are exactly the same as in the Fourier basis—but the Fourier-Bessel basis is optimal, in the sense that it does not keep track of irrelevant modes, only the ones that contribute constructively to the physical observables.

The previous discussion implies that our results and methods are suitable for analytical and numerical studies of CMB temperature and polarization maps in models with large-scale inhomogeneities, statistical anisotropy or non-Gaussianities of any kind [29–32]. Our results may be useful also in simulations of the CMB in the presence of topological defects. It is not clear whether the methods described here can be employed to study models with nontrivial topology [33], since in those cases the Fourier or Fourier-Bessel basis functions may not be eigenvectors of the Laplace-Beltrami operator.

ACKNOWLEDGMENTS

The authors would like to thank J. C. A. Barata for many conversations on the properties of Bessel functions, and to Mathias Zaldarriaga for useful comments. This work was supported by FAPESP and CNPq.

APPENDIX: INTEGRALS OF BESSEL FUNCTIONS

1. Integral of products of spherical Bessel functions

We will now compute the integrals of spherical Bessel functions that were presented in Sec. III to obtain the spacetime window functions. Parts of the methods used here can be found in [28]. The results below also provide the motivation for the diagrammatic representation of the window functions shown in Fig. 3.

The spherical Bessel functions are associated with the matrix elements of the Euclidean group in three dimensions, E_3 [44]. The Euclidean group E_3 consists of the set of transformations that leaves spatial distances invariant—i.e., spatial translations and rotations. The rules of group multiplication lead to addition theorems for the special functions which realize the group representation, one example of which is the orthogonality condition of Eq. (18). Although E_3 is not compact, the spherical Bessel functions also obey an addition rule, namely [44]:

$$\frac{j_m(kr)}{(kr)^m} = \sum_{n=m}^{\infty} \frac{(2n+1) j_n(kr_1) j_n(kr_2)}{[(kr_1)(kr_2)\sin\alpha]^m} P_n^{(m)}(\cos\alpha), \quad \text{(A1)}$$

where (r, r_1, r_2) form a triangle and α is the angle between sides r_1 and r_2.

2. Integral of three spherical Bessel functions

We can use Eq. (A1) and the orthogonality of Legendre polynomials,

$$\int_{-1}^{1} dx P_\ell^{(m)}(x) P_{\ell'}^{(-m)}(x) = (-1)^m \frac{2}{2\ell+1} \delta_{\ell,\ell'}, \quad \text{(A2)}$$

to reduce the product of two Bessel functions to only one Bessel function. Choosing $m = 2$ due to the demands of our particular problem, we have

$$\begin{aligned} j_\ell(kr_1) j_\ell(kr_2) &= \sum_{\ell'=2}^{\infty} j_{\ell'}(kr_1) j_{\ell'}(kr_2) \delta_{\ell,\ell'} \\ &= \sum_{\ell'=2}^{\infty} \frac{2\ell'+1}{2} \int_{-1}^{1} d(\cos\alpha) j_{\ell'}(kr_1) j_{\ell'}(kr_2) \\ &\quad \times P_\ell^{(2)}(\cos\alpha) P_{\ell'}^{(-2)}(\cos\alpha) \\ &= \frac{1}{2} \int_{-1}^{1} d(\cos\alpha) P_\ell^{(-2)}(\cos\alpha) (kr_1)^2 (kr_2)^2 \\ &\quad \times \sin^2\alpha \sum_{\ell'=2}^{\infty} \\ &\quad \times \frac{(2\ell'+1) j_{\ell'}(kr_1) j_{\ell'}(kr_2) P_{\ell'}^{(2)}(\cos\alpha)}{[(kr_1)(kr_2)\sin\alpha]^2}. \end{aligned} \quad \text{(A3)}$$

Now we perform a change of variable, calling r the side of the triangle whose other two sides are r_1 and r_2, such that α is the angle between r_1 and r_2, i.e. $r^2 = r_1^2 + r_2^2 - 2r_1 r_2 \cos\alpha$. Performing this change of variables, we obtain

$$\int_{-1}^{1} d(\cos\alpha) \to \int_{|r_1 - r_2|}^{r_1 + r_2} dr \frac{r}{r_1 r_2},$$

and therefore

$$j_\ell(kr_1) j_\ell(kr_2) = \frac{1}{2} \int dr k^2 \frac{r_1 r_2}{r} j_2(kr) P_\ell^{(-2)}(\cos\alpha) \sin^2\alpha. \quad \text{(A4)}$$

Consider, then, the integral that is relevant to us

$$\int dk j_\ell(kr_1) j_\ell(kr_2) j_2(kr_3) = \frac{r_1 r_2}{2} \int \frac{dr}{r} P_\ell^{(-2)}(\cos\alpha) \sin^2\alpha \times \int dk k^2 j_2(kr) j_2(kr_3). \quad \text{(A5)}$$

But now we can employ the orthogonality of Bessel functions, Eq. (18), so that the k integral gives $(\pi/2) r^{-2} \delta(r - r_3)$ and the radial integral can be computed to arrive at the final expression

$$I_\ell^{(3)}(r_1, r_2, r_3) = \int dk j_\ell(kr_1) j_\ell(kr_2) j_2(kr_3) = \frac{\pi}{4} \frac{r_1 r_2}{r_3^3} P_\ell^{(-2)}(\cos\alpha) \sin^2\alpha, \quad \text{(A6)}$$

where r_1, r_2, and r_3 must form a triangle: if they do not, the radial integral yields zero because then r_3 cannot be equal to some r which, by assumption, forms a triangle together with r_1 and r_2. Identifying $r_1 \to x$, $r_2 \to \Delta\eta$, and $r_3 \to \Delta\eta'$ we obtain the result shown in Eq. (21). This integral is also computed in [28], in a more general case but employing other methods.

For the series representation of the window function, consider Eq. (44). The same trick that was shown above, i.e., to exchange two spherical Bessel functions for an integral over a Legendre polynomial, can be used to obtain

$$\sum_i \frac{j_\ell(k_{i\ell} r_1) j_\ell(k_{i\ell} r_2) j_2(k_{i\ell} r_3)}{k_{i\ell}^2 j_{\ell+1}^2(k_{i\ell} R)} = \frac{r_1 r_2}{2} \int \frac{dr}{r} P_\ell^{(-2)}(\cos\alpha) \sin^2\alpha \frac{1}{r} \sum_i \frac{j_2(k_{i\ell} r_3) j_2(k_{i\ell} r)}{j_{\ell+1}^2(k_{i\ell} R)}. \quad \text{(A7)}$$

Using now the conjectured orthogonality relation, Eq. (45), with $\ell' = 2$, we obtain that the window function of Eq. (44) is indeed identical to the window function of Eq. (21).

3. Integration of four spherical Bessel functions

Consider now the integral that appears in the case of $N = 2$ scatterings:

$$I_\ell^{(4)} = \int_0^\infty dk k^{-2} j_\ell(kr_1) j_\ell(kr_2) j_2(kr_3) j_2(kr_4). \quad \text{(A8)}$$

To benefit from the results obtained above for the case of the integral of three Bessel functions, let α_{12} be the angle formed by r_1 and r_2, i.e., $r^2 = r_1^2 + r_2^2 - 2 r_1 r_2 \cos\alpha_{12}$, and use Eq. (A1) to rewrite Eq. (A8) as

$$I_\ell^{(4)} = \frac{r_1 r_2}{2} \int_{|r_1 - r_2|}^{r_1 + r_2} \frac{dr}{r} P_\ell^{-2}(\cos\alpha_{12}) \sin^2\alpha_{12} \times \int_0^\infty dk j_2(kr_3) j_2(kr_4) j_2(kr) = \frac{r_1 r_2}{2} \int_{|r_1 - r_2|}^{r_1 + r_2} \frac{dr}{r} P_\ell^{-2}(\cos\alpha_{12}) \sin^2\alpha_{12} \times I_2^{(3)}(r_3, r_4, r) \quad \text{(A9)}$$

The integral $I_2^{(3)}$ of three spherical Bessel functions of order two is a symmetric case of Eq. (A6), and it vanishes unless r, r_3, and r_4 are the sides of a triangle. In this case we can choose any angle in the triangle, so to be consistent let us choose that to be the angle between r_3 and r_4, that is, $r^2 = r_3^2 + r_4^2 - 2 r_3 r_4 \cos\alpha_{34}$. Since r_1, r_2, and r must also form a triangle, r and the angle α_{34} will be determined in terms of r_1, r_2, r_3, r_4, and α_{12}. The final answer is, therefore, given by

$$I_\ell^{(4)}(r_1, r_2, r_3, r_4) = \frac{\pi}{8} r_1 r_2 r_3 r_4 \int_G \frac{dr}{r^4} P_\ell^{(-2)}(\cos\alpha_{12}) \times \sin^2\alpha_{12} P_2^{(-2)}(\cos\alpha_{34}) \sin^2\alpha_{34} \quad \text{(A10)}$$

where G is the range of values allowed for r under the conditions that both the triangle of sides (r_1, r_2, r) and the one with sides (r_3, r_4, r) exist. These conditions are simply the set of inequalities that guarantee that the polygon of sides (r_1, r_2, r_3, r_4) can exist, i.e., $r_1 \le r_2 + r_3 + r_4$ and the three other cyclical permutations of that inequality. The two triangles that must be formed so that Eq. (A8) does not vanish are shown in Fig. 3. This result was used in our Eq. (28).

4. The general case

Our problem deals with the propagation of signals between points (events) in spacetime. The first signal propagates freely from the source to the point where the photon first scatters, and then there is a set of propagations from one scattering to the next, until finally there is a propagation term from the point where the photon have last scattered to the point where it is observed. The propagation from the source to the first scattering correspond to a term $j_2(k\Delta\eta_1)$ and each propagation between scatterings to $j_2(k\Delta\eta_i)/(k\Delta\eta_i)^2$. The propagation from the last scattering to the observation point corresponds to a term $j_\ell(k\Delta\eta_N)/(k\Delta\eta_N)^2$. Besides these propagation terms, the Hankel transforms (which were used to go back from Fourier to position space) introduce a $j_\ell(kx)$ into our integral.

Therefore, for N scatterings we will get integrals over k with an integrand having the following features:

(i) two Bessel functions of order ℓ, of arguments kr_1 and kr_2 (by convention);
(ii) N spherical Bessel functions of order 2, of arguments $kr_3, \ldots, kr_{N+2}$;

(iii) a factor of $k^{-2}k^{-2(N-2)} = k^{-2(N-1)}$

The method that was used above to compute the integrals in the cases $N = 1$ and $N = 2$ takes advantage of the fact that we can exchange pairs of spherical Bessel functions for Legendre polynomials and radial (or angular) integrals. Now, we can do this for every pair of Bessel functions in the N-scattering integral: if that number is even, every Bessel function can be exchanged for an integral over a Legendre polynomial; if that number is odd, an extra Bessel function will appear. The final integral over k can then be computed with the help of the lower order integrals.

For $N = 3$ this procedure leads to

$$I_\ell^{(5)} = \int dk k^{-4} j_\ell(kr_1) j_\ell(kr_2) j_2(kr_3) j_2(kr_4) j_2(kr_5) = \frac{r_1 r_2 r_3 r_4}{2^2} \int \frac{dr_{12}}{r_{12}} \int \frac{dr_{34}}{r_{34}} P_\ell^{(-2)}(\cos\alpha_{12}) \sin^2\alpha_{12} \times P_2^{(-2)}(\cos\alpha_{34}) \sin^2\alpha_{34} I_2^{(3)}(r_{12}, r_{34}, r_5), \quad \text{(A11)}$$

where r_{34} makes a triangle together with r_3 and r_4, and the angles are clearly indicated with respect to their respective sides. Notice that, as opposed to the case $N = 2$, when the sides and the angle α_{12} uniquely determines the remaining angle of that four-side polygon, in the case $N = 3$ the triangle of sides (r_3, r_4, r_{34}) is totally free to acquire many shapes—see also Fig. 3. It is only when both α_{12} and α_{34} are given that the angle between r_{12} and r_{34} is fixed.

It is also instructive to look at the case $N = 4$, for the integral of six Bessel functions. In that case we have

$$I_\ell^{(6)} = \int dk k^{-6} j_\ell(kr_1) j_\ell(kr_2) j_2(kr_3) j_2(kr_4) j_2(kr_5) j_2(kr_6) = \frac{r_1 r_2 r_3 r_4 r_5 r_6}{2^3} \int \frac{dr_{12}}{r_{12}} \int \frac{dr_{34}}{r_{34}} \int \frac{dr_{56}}{r_{56}} \times P_\ell^{(-2)}(\cos\alpha_{12}) \times \sin^2\alpha_{12} P_2^{(-2)}(\cos\alpha_{34}) \sin^2\alpha_{34} P_2^{(-2)}(\cos\alpha_{56}) \times \sin^2\alpha_{56} I_2^{(3)}(r_{12}, r_{34}, r_{56}). \quad \text{(A12)}$$

The expressions for $I_\ell^{(7)}$ and $I_\ell^{(8)}$ can be obtained in terms of $I_\ell^{(4)}$; and so on. With these methods it is trivial to compute the spacetime window functions for an arbitrary number of scatterings.

The set of conditions under which the integrals above are different from zero are those that ensure that each internal triangle (corresponding to each instance where two Bessel functions were exchanged for a Legendre polynomial and a Bessel function) exist. So, for $\ell = 4$ we would impose

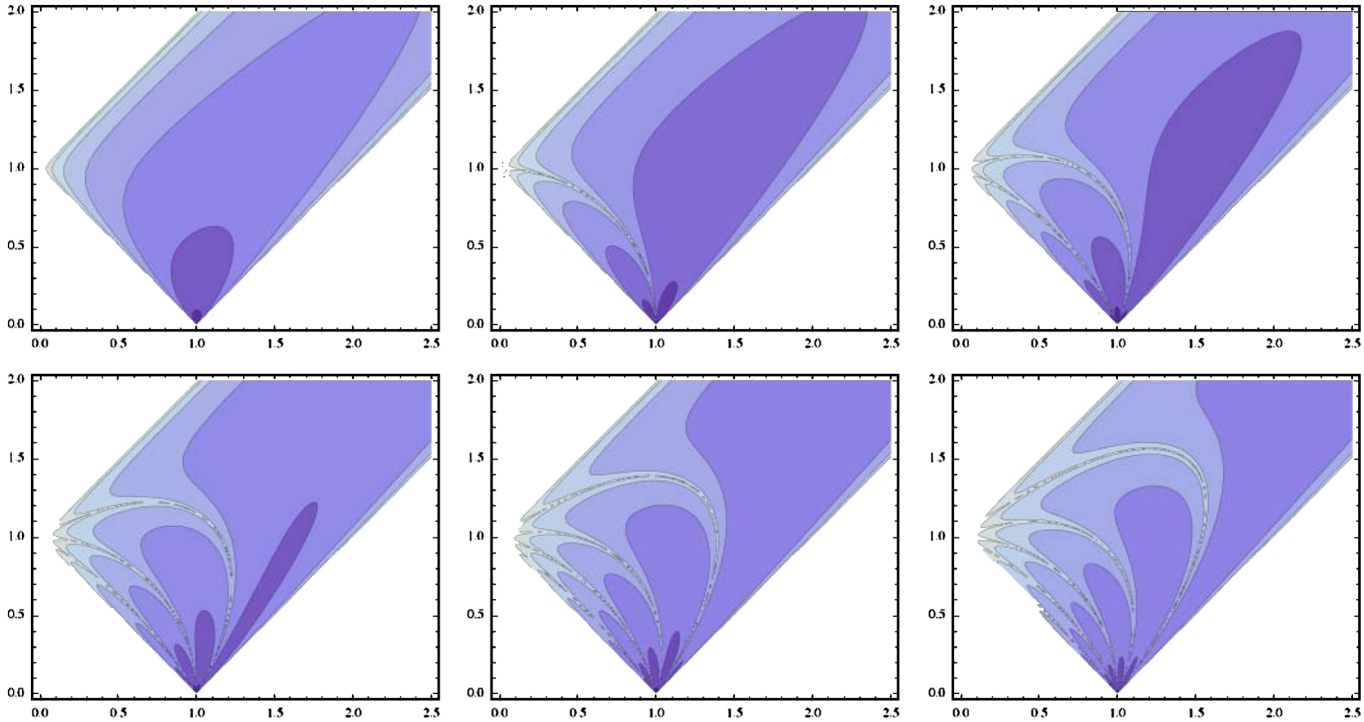

FIG. 5 (color online). Contour plots of the window functions $W_\ell^3(x, \Delta\eta; 1)$ for the cases $\ell = 2, 3, 4$ (top panels, left to right panels), and 5, 6, and 7 (bottom panels.) In these plots x (the radial position of the sources) corresponds to the horizontal axes, and $\Delta\eta = \eta - \eta'$ corresponds to the vertical axes. For visualization purposes we have fixed $\Delta\eta' = \eta' - \eta'' = 1$. Physically, this corresponds to taking sources at positions x and times η'', and photons which scatter at times η' before they are observed at time η. For visualization purposes we plotted $\log|W_\ell^3(x, \Delta\eta; 1)|$, so large absolute values of the window functions are indicated by darker hues, and the window functions vanish in the white areas. Each lobe corresponds to intercalating negative and positive values of the window function.

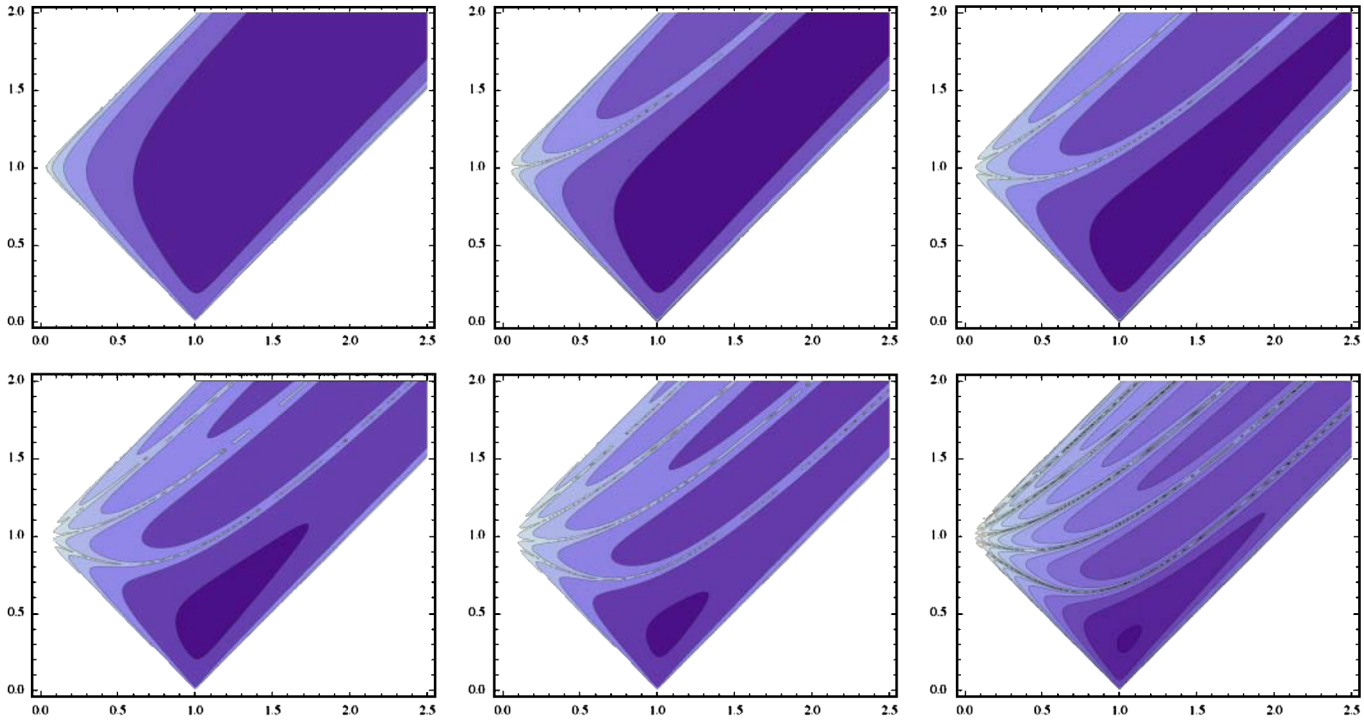

FIG. 6 (color online). Same as above, but now we fix $\Delta\eta = \eta - \eta' = 1$ so the contour plots correspond to $W_\ell^3(x, 1; \Delta\eta')$ for the cases $\ell = 2$, 3, 4 (top panels, left to right panels), and 5, 6, and 7 (bottom panels.) Now $\Delta\eta'$ corresponds to the vertical axes, and x corresponds to the horizontal axes.

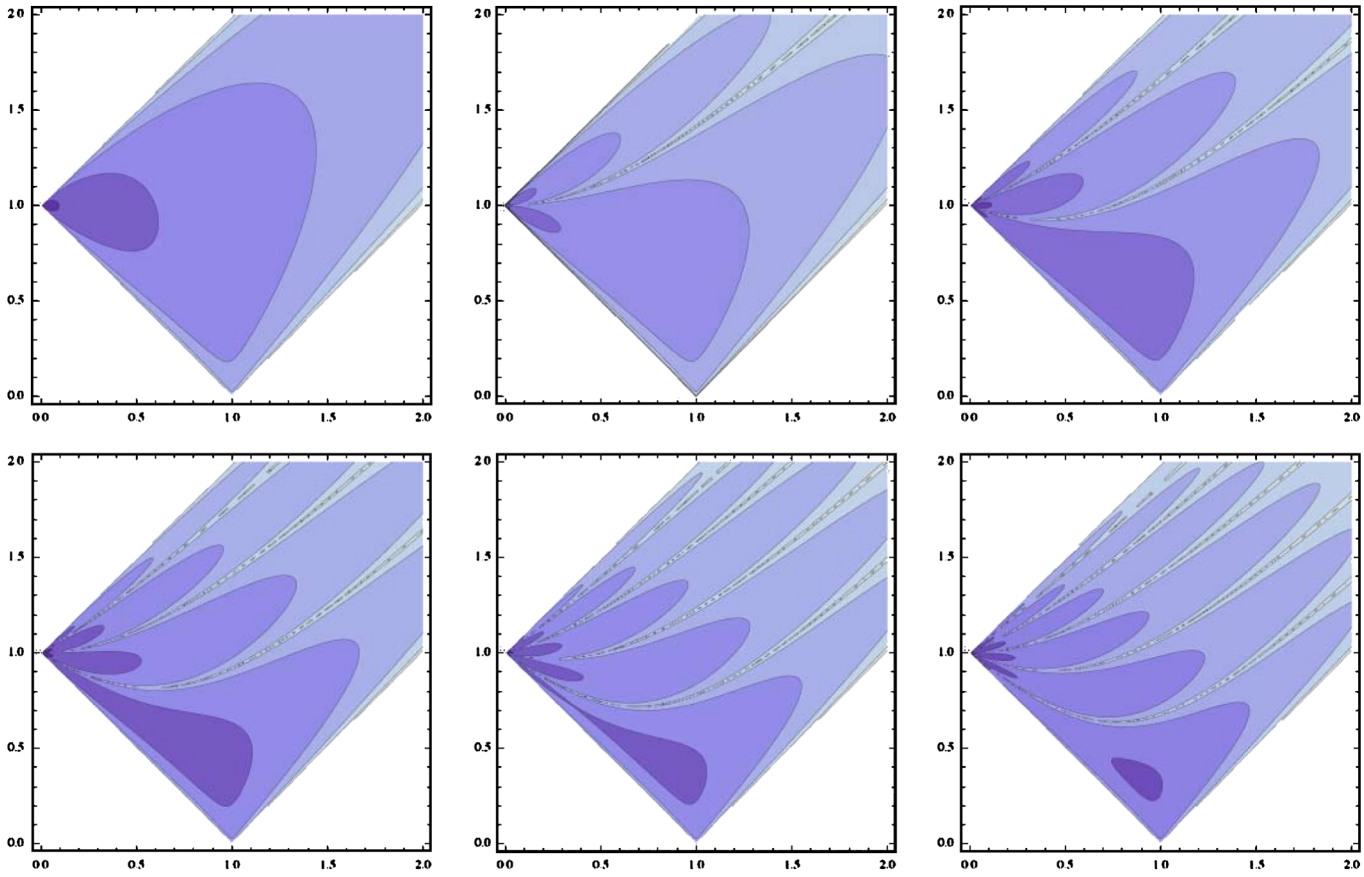

FIG. 7 (color online). Same as above, but now we fix $x = 1$, so the contour plots correspond to $W_\ell^3(1, \Delta\eta; \Delta\eta')$ for the cases $\ell = 2$, 3, 4 (top panels, left to right panels), and 5, 6, and 7 (bottom panels.) $\Delta\eta$ corresponds to the horizontal axes, and $\Delta\eta'$ to the vertical axes.

$$r_1 \le r_2 + r_{12}, \qquad r_2 \le r_{12} + r_1, \qquad r_{12} \le r_1 + r_2,$$
$$r_3 \le r_4 + r_{34}, \qquad r_4 \le r_{34} + r_3, \qquad r_{34} \le r_3 + r_4.$$

With the additional condition that $r_{12} = r_{34}$ in the case $\ell = 4$ (see the discussion in A 3), it is trivial to verify that these conditions reduce to the inequalities (29).

The set of conditions above simply tells us that the four-sided polygon of Fig. (3) exists—in other words, that one can form a closed polygon with those sides. For any ℓ the resulting set of conditions ensure that a flat polygon with the sides given by $r_1, \ldots, r_N$ exists, i.e.

$$r_1 \le r_2 + \ldots + r_N,$$

and all cyclical permutations. These inequalities constitute a simple set of constraints that, if not satisfied, imply that the spacetime window functions W_ℓ^N vanish identically. This simplifies tremendously the integration of the sources over time in position space. In particular, one of these inequalities implies that

$$x \le \Delta\eta_1 + \ldots + \Delta\eta_{N-1} = \eta - \eta_N,$$

which means that all the sources that contribute to the observables are located at radii x which are *inside* the past light cone of the observation point at time η, all the way to the time η_N when those sources were evaluated, N scatterings prior to the observation.

5. Spacetime window function W_ℓ^3

The spacetime window functions regulate how sources at some position x contribute to the observables at time η. For the case of one scattering (order γ), the window function is a δ-function on the PLC, $\delta(x - \Delta\eta)$, where $\Delta\eta = \eta - \eta'$ and η' is the time of the scattering.

For two scatterings (order γ^2), the window function is nonvanishing inside the PLC. In Figs. 5–7 we show a few examples of the window functions $W_\ell^3(x, \Delta\eta; 1)$.

[1] G. F. Smoot *et al.*, Astrophys. J. **396**, L1 (1992).
[2] C. L. Bennett *et al.* (WMAP), Astrophys. J. Suppl. Ser. **148**, 1 (2003).
[3] D. N. Spergel *et al.* (WMAP), Astrophys. J. Suppl. Ser. **148**, 175 (2003).
[4] E. Komatsu *et al.*, arXiv:1001.4538.
[5] L. Page *et al.* (WMAP), Astrophys. J. Suppl. Ser. **170**, 335 (2007).
[6] M. L. Brown *et al.* (QUaD), Astrophys. J. **705**, 978 (2009).
[7] H. C. Chiang *et al.*, Astrophys. J. **711**, 1123 (2010).
[8] S. Dodelson, *Modern Cosmology* (Academic Press, New York, 2003).
[9] V. Mukhanov, *Physical Foundations of Cosmology* (Cambridge University Press, Cambridge, England, 2005).
[10] R. Durrer, *The Cosmic Microwave Background* (Cambridge University Press, Cambridge, England, 2008).
[11] P. Peter and J.-P. Uzan, *Primordial Cosmology* (Oxford University Press, New York, 2009).
[12] S. Chandrasekhar, *Radiative Transfer* (Dover, New York, 1960).
[13] P. J. E. Peebles and J. T. Yu, Astrophys. J. **162**, 815 (1970).
[14] J. R. Bond and G. Efstathiou, Mon. Not. R. Astron. Soc. **226**, 655 (1987).
[15] J. R. Bond and G. Efstathiou, Astrophys. J. **285**, L45 (1984).
[16] C.-P. Ma and E. Bertschinger, Astrophys. J. **455**, 7 (1995).
[17] W. Hu and N. Sugiyama, Astrophys. J. **471**, 542 (1996).
[18] W. Hu, N. Sugiyama, and J. Silk, Nature (London) **386**, 37 (1997).
[19] U. Seljak and M. Zaldarriaga, Phys. Rev. Lett. **78**, 2054 (1997).
[20] M. Zaldarriaga and U. Seljak, Phys. Rev. D **55**, 1830 (1997).
[21] M. Kamionkowski, A. Kosowsky, and A. Stebbins, Phys. Rev. Lett. **78**, 2058 (1997).
[22] M. Kamionkowski, A. Kosowsky, and A. Stebbins, Phys. Rev. D **55**, 7368 (1997).
[23] W. Hu and M. J. White, Phys. Rev. D **56**, 596 (1997).
[24] W. Hu, U. Seljak, M. J. White, and M. Zaldarriaga, Phys. Rev. D **57**, 3290 (1998).
[25] U. Seljak and M. Zaldarriaga, Astrophys. J. **469**, 437 (1996).
[26] J. J. Sakurai, *Advanced Quantum Mechanics* (Addison Wesley, Reading, MA, 1967).
[27] R. K. Sachs and A. M. Wolfe, Astrophys. J. **147**, 73 (1967).
[28] G. N. Watson, *A Treatise on the Bessel Functions* (Cambridge University Press, Cambridge, England, 1944).
[29] M. Liguori, S. Matarrese, and L. Moscardini, Astrophys. J. **597**, 57 (2003).
[30] E. Komatsu, D. N. Spergel, and B. D. Wandelt, Astrophys. J. **634**, 14 (2005).
[31] M. Liguori *et al.*, Phys. Rev. D **76**, 105016 (2007).
[32] F. Elsner and B. D. Wandelt, Astrophys. J. Suppl. Ser. **184**, 264 (2009).
[33] N. J. Cornish, D. N. Spergel, G. D. Starkman, and E. Komatsu, Phys. Rev. Lett. **92**, 201302 (2004).
[34] S. Bashinsky and E. Bertschinger, Phys. Rev. Lett. **87**, 081301 (2001).
[35] S. Bashinsky and E. Bertschinger, Phys. Rev. D **65**, 123008 (2002).
[36] A. Kosowsky, Ann. Phys. (N.Y.) **246**, 49 (1996).
[37] N. Straumann, Ann. Phys. (Leipzig) **15**, 701 (2006).
[38] L. R. Abramo and H. S. Xavier, Phys. Rev. D **75**, 101302

(2007).
[39] A. J. S. Hamilton and M. Culhane, Mon. Not. R. Astron. Soc. **278**, 73 (1996).
[40] A. F. Heavens and A. N. Taylor, Mon. Not. R. Astron. Soc. **275**, 483 (1995).
[41] A. J. S. Hamilton, arXiv:astro-ph/9708102.
[42] E. F. Bunn, Phys. Rev. D **73**, 123517 (2006).
[43] M. Kamionkowski and A. Loeb, Phys. Rev. D **56**, 4511 (1997).
[44] J. D. Talman, *Special Functions: A Group Theoretic Approach* (Benjamin, New York, 1968).
[45] J. M. Maldacena, J. High Energy Phys. 05 (2003) 013.